Petrological and Mineralogical Aspects of Epithermal Low-Sulfidation Au- and Porphyry Cu-Style Mineralization, Navilawa Caldera, Fiji

Nathan A. Forsythe [1], **Paul G. Spry** [1,*] and **Michael L. Thompson** [2]

[1] Department of Geological and Atmospheric Sciences, Iowa State University, Ames, IA 50011, USA; n4sythe@gmail.com
[2] Department of Agronomy, Iowa State University, Ames, IA 50011, USA; mlthomps@iastate.edu
[*] Correspondence: pgspry@iastate.edu; Tel.: +1-515-294-9637

Abstract: The Navilawa caldera is the remnant of a shoshonitic volcano on Viti Levu, Fiji, and sits adjacent to the low-sulfidation Tuvatu epithermal Au–Te deposit. The caldera occurs along the Viti Levu lineament, approximately 50 km SW of the Tavua caldera, which hosts the giant low-sulfidation Emperor epithermal Au–Te deposit. Both calderas host alkaline rocks of nearly identical age (~5.4–4.6 Ma) and mineralization that occurred in multiple stages. The gold mineralization in these locations is spatially and genetically related to monzonite intrusions and low-grade porphyry Cu-style mineralization. Potassic, propylitic, phyllic, and argillic alteration extends from the Tuvatu Au–Te deposit towards the central, northern, and eastern parts of the Navilawa caldera where it is spatially associated with low-grade porphyry Cu–Au mineralization at the Kingston prospect and various epithermal Au–(Te) vein systems, including the Banana Creek and Tuvatu North prospects. Chalcopyrite, and minor bornite, occurs in quartz–calcite–(adularia) veins in the Kingston deposit associated with weak propylitic and phyllic alteration, whereas NE-trending epithermal gold veins at the Banana Creek and Tuvatu North prospects are associated with weak potassic alteration that is overprinted by propylitic and phyllic alteration. Gold is accompanied by chalcopyrite, galena, and sphalerite in quartz–pyrite veins that also have a Ag–As–Hg–Te signature. The temperature range for phyllosilicates in the phyllic alteration (chlorite ± smectite ± corrensite ± illite) is in good agreement with temperatures recorded from previous fluid inclusion studies of quartz at the Banana Creek Au prospect (~260 °C) and the nearby Tuvatu Au–Te deposit (205 to 382 °C). Sulfur isotope compositions of pyrite (-6.2 to $+0.4$‰) from the Banana Creek prospect indicate a likely magmatic source of sulfur. Oxidation of the ore fluids or a direct addition of volatiles to the hydrothermal fluids may account for the lighter isotopic values. The similarities of the igneous rock types and compositions, transition from porphyry- to epithermal-style mineralization, alteration assemblages, paragenetic relationships, and stable isotope data suggest a common origin for the porphyry- and epithermal-style mineralization within the Navilawa and between the Navilawa and Tavua calderas.

1. Introduction

A spatial and genetic relationship exists between low-sulfidation gold deposits and alkaline igneous rocks [1–3], especially in the southwest Pacific in the Acupan, [4], Porgera, [5,6], Mt. Kare [7], Ladolam [8], Emperor [9], and Tuvatu [10] deposits. Of these deposits, there is a notable association among epithermal gold mineralization, a volcanic caldera, and regional tectonic lineaments at the Emperor [11–14] and Ladolam [8] deposits.

A regional gravity survey shows strong bullseye gravity anomalies >20 km in diameter that correlate with the position of four volcanic calderas in the northwestern part of the island of Viti Levu, Fiji: Tavua, Rakiraki, Ba, and Navilawa [15,16]. Each of these calderas is spatially associated with epithermal gold mineralization and occurs along the prominent regional Viti Levu lineament [17]. The large Emperor Au–Te deposit (280 t Au) occurs on the western side of the Tavua volcano [9,11], but there is also a genetic relationship to low-grade porphyry Cu mineralization, which occurs beneath the Emperor deposit [11] and within the Tavua caldera [18,19]. As was shown by Scherbarth and Spry [10], there are similar igneous rocks of comparable age, a transition from epithermal- to porphyry-style mineralization, paragenetic relationships among vein types, alteration types, and conditions of ore formation between the Emperor and Tuvatu deposits, the latter of which is the second largest gold deposit in Fiji (~13 t Au). The Tuvatu Au–Te deposit, which occurs approximately 50 km southeast of Emperor, is one of several epithermal gold telluride and low-grade porphyry Cu prospects that occur in or on the margins of the Navilawa caldera [17].

The low-grade Kingston porphyry Cu–Au prospect occurs near the center of the Navilawa caldera whereas the Banana Creek and Tuvatu North Au prospects occur on its eastern and southern sides, respectively. North-northeast-trending and E–W-trending faults in the Navilawa caldera, which are similar in orientation to the major faults in the Tavua caldera, coupled with the presence of potassic, propylitic, sericitic, and phyllic alteration in both calderas, suggest similarities between the hydrothermal mineralization spatially associated with the Tavua and Navilawa calderas [17]. The exploration potential for further gold-telluride mineralization in the Navilawa caldera is apparent.

In 2007 and 2008, Golden Rim Resources Ltd. drilled three holes at the Banana Creek prospect and four at the Tuvatu North prospect in the Navilawa caldera that were located, in large part, on the basis of results derived from helicopter-borne magnetic and potassium radiometric anomalies, mapping, and rock chip sampling (www.goldenrim.com.au). Exploration leases within the caldera are currently controlled by Lion One Metals Limited. The objective of the present study is to extend the petrological, geochemical, and mineralogical study of Scherbarth and Spry [10] to the north of the Tuvatu prospect and within the center of the Navilawa caldera. Surface samples were collected initially as part of this study, but due to the high degree of surface weathering, samples were subsequently obtained from the holes drilled by Golden Rim Resources Ltd. Although a preliminary study of the alteration assemblages was previously made at the Tuvatu [11] deposit, the current study has focused on the different types of alteration in the Banana Creek and Tuvatu North prospects. A preliminary microscope study of thin sections here made it apparent that an understanding of the distribution of phyllosilicates in the alteration associated with epithermal-style mineralization was essential if the distribution of alteration types was to be useful in exploring for additional epithermal-style mineralization in the Navilawa caldera. The study of phyllosilicate mineralogy has been used previously in the exploration for porphyry copper and epithermal gold mineralization [19–24]. The main aim of the present study is to evaluate the petrology and mineralogy of the Banana Creek and Tuvatu North epithermal Au deposits, as well as the Kingston Cu–Au prospect, to determine whether these prospects are similar to porphyry- and epithermal-style prospects in the Tavua caldera, and the Tavuta deposit on the margin of the Navilawa caldera. Sulfur isotope compositions of pyrite from the Banana Creek prospect obtained here are compared to those obtained previously from the Tuvatu [10] and Emperor [9,11] deposits.

2. Geological Setting

2.1. Regional Geology

Fiji is an archipelago of approximately 300 islands, the largest being Viti Levu and Vanua Levu. The islands are positioned on an offset of the convergent boundary between the Pacific and Indo-Australian tectonic plates known as the Fiji Platform. In this area, plate boundaries are discontinuous with subduction occurring westward at the Tonga arc and reversing to eastward subduction at New Hebrides [25]. The NE-trending Hunter Fracture Zone (HFZ) and the ENE-trending

Fiji Fracture Zone (FFZ) continue to be active, major left-lateral transform zones. The FFZ defines the northern boundary of the Fiji Platform whereas the former is a fossil subduction zone where the South Fiji Basin was being subducted beneath Fiji [25,26].

Three lineaments subparallel to the FFZ appear to have controlled the distribution of Late Miocene–Early Pliocene volcanic centers on the Fiji Platform [26]. The Viti Levu lineament, which extends from northwest Viti Levu through Vanua Levu, is associated with seven shoshonitic and calc–alkaline volcanic centers, the largest being the Tavua caldera located on Viti Levu. The Lomaiviti and Vatulele–Beqa lineaments, east and south of Viti Levu respectively, are represented by island chains on the margins of the Fiji Platform and dominated by Pliocene shoshonitic and calc–alkaline volcanism [14].

The magmatic compositions changed from island arc tholeiites and calc–alkaline andesites to shoshonites at ~5.5 Ma [26]. The oldest rocks are the Upper Eocene to Lower Oligocene Yavuna Group (35–40 Ma), which occur along the western portion of Viti Levu. They are composed of extrusive and intrusive tholeiitic basalts, a trondhjemitic stock, and other minor volcaniclastic rocks and limestones [27]. The Yavuna Group is separated by an unconformity to the Lower Oligocene to Middle Miocene Wainimala Group (13–32 Ma), which outcrops in southern Viti Levu and on smaller islands to the west. The Wainimala Group is mostly volcaniclastic rudites and lavas, but it also consists of shallow water limestones and a basinal assemblage, which includes volcaniclastic turbidites, hemipelagic carbonates, and tuffs [11,27].

During the Middle to Late Miocene (12.5–7 Ma), the Colo Orogeny occurred, creating large scale faulting and folding of the Wainimala Group. This orogenic event also emplaced a plutonic suite of gabbro and minor tonalite intrusions, which occur in a semi-continuous belt from southwestern to eastern Viti Levu [11,14]. At the end of the Colo Orogeny, Viti Levu underwent a period of widespread volcanism from 6.5 Ma to 2.5 Ma [17]. Several sedimentary packages (Medrausucu, Nadi, Tuva, Navosa, Cuvu, and Ra Groups) were deposited on Viti Levu during the Upper Miocene to Lower Pliocene as a result of erosion from the calc–alkaline volcanics and rocks of the Wainimala-Colo Group [28].

During the Early Pliocene, a shift in the volcanic activity to the northern portions of Viti Levu occurred. This activity produced the Tavua, Vuda, and Rakiraki volcanoes, which are composed of shoshonite and high-K calc–alkaline volcanic rocks [17]. The Ba Volcanic Group dominates the northern half of Viti Levu and is composed of shoshonites and a lesser extent of calc–alkaline volcanics. The Tavua volcano is the main feature of the Ba Volcanic Group and hosts the Emperor gold deposit [11]. The Koroimavua Group occurs to the northeast of Nadi and consists of shoshonitic volcaniclastic sandstones and mudstones overlain by the Sabeto Volcanics, which include shoshonitic lavas, breccias, rudites, and sandstones. Both the Ba and Koroimavua Groups occur along the ENE-trending axis, which defines the Viti Levu lineament, and appear to be contemporaneous (Figure 1).

2.2. Local Geology

The Navilawa caldera is approximately 4 km in diameter and cross-cut by the Upper Sabeto River Valley. It is located 21 km NE of Nadi, the third-largest township in Fiji, and it is dominated by cliffs of the Mt. Evans Range, which are interpreted to be the eroded remnants of the caldera. The cliffs form an arena around Navilawa village, rising to a height of ~1300 m [29]. The Tuvatu deposit lies along the southwest margin of the caldera. The Nadele Breccia, which is a member of the Wainimala Group, is the oldest geologic unit dated at 12–26 Ma. It consists of volcanic, polymict, epiclastic breccia, pyroclastic rocks and minor flows [30]. The Nadele Breccia contains zeolite, chlorite, and epidote within the groundmass, which formed due to zeolite and greenschist facies metamorphism during the Colo Orogeny.
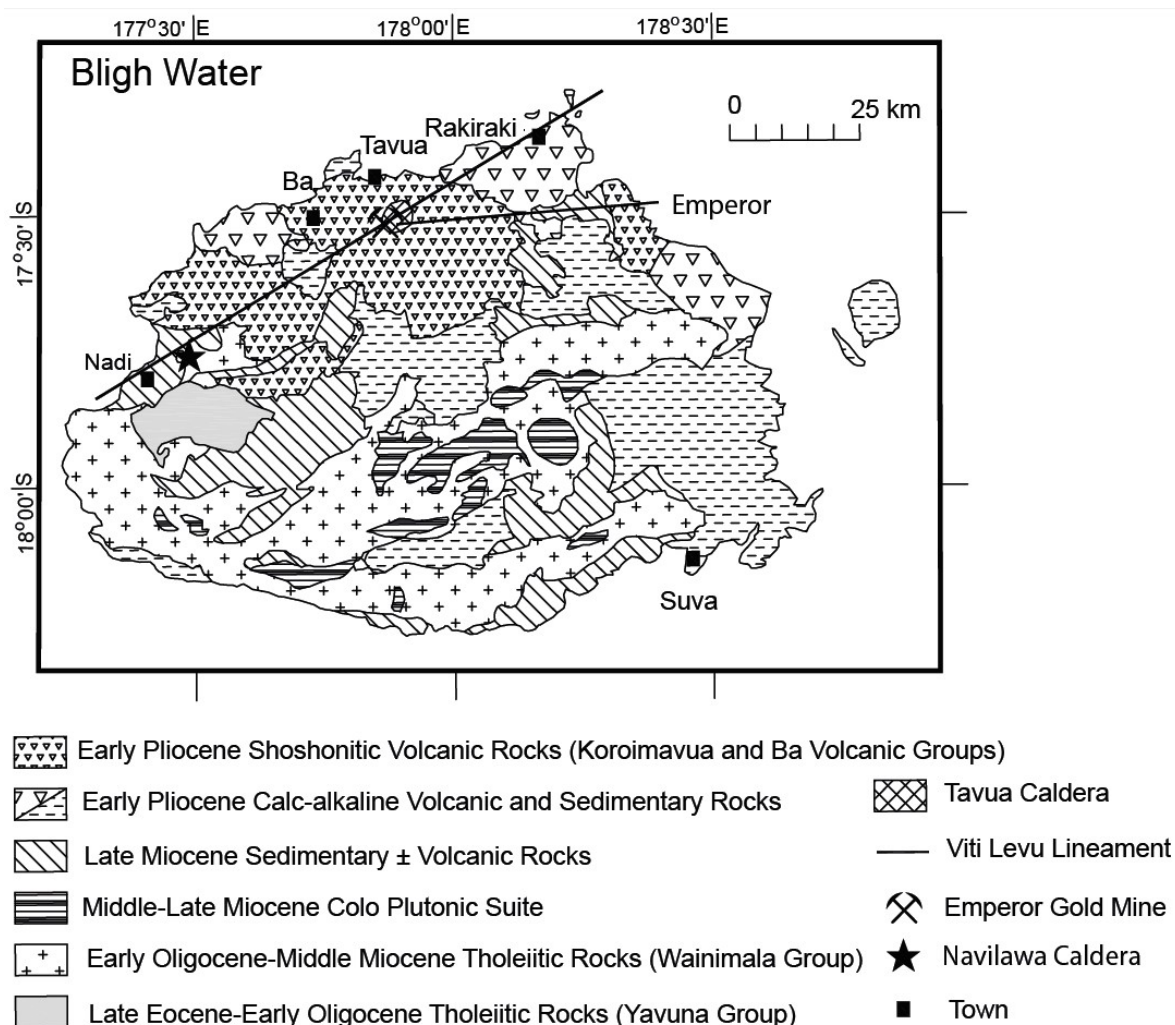
Figure 1. Geology of Viti Levu, Fiji (modified from [10,11,31]). The locations of the Navilawa and Tavua calderas relative to the Emperor deposit and the Viti Levu lineament are shown.

The Wainimala Group is unconformably overlain by the subgroup Sabeto Volcanics of the Koroimavua Volcanic Group. Dating of the Sabeto Volcanics, which are comprised of augite–biotite flows and breccia with a basal sequence of andesitic and dacitic lithic and crystal tuffs, grits and agglomerates with minor flows, yielded a K-Ar age of 5.35 Ma [30,32]. The 4.85 Ma Navilawa Monzonite intruded the latter two geological units in the center of the caldera and is interpreted to be the intrusive equivalent of the Koroimavua Volcanic Group [32]. The Navilawa Monzonite consists of multiple phases of intrusions including an early micromonzonite, a medium-grained monzonite, basaltic–andesite dikes, and late-stage pegmatitic dikes [33]. Ricketts et al. [34] distinguished two lithological variations of the Navilawa Monzonite intrusion. The first variant contains medium- to coarse-grained plagioclase, potassium feldspar, augite, and biotite with minor quartz, carbonate, epidote, iron oxides, magnetite, and pyrite. The second unit is a monzonite porphyry comprised of potassium feldspar and augite phenocrysts in a fine- to medium-grained groundmass of potassium feldspar and plagioclase with minor augite, biotite, pyrite, and iron oxides.

Porphyry Cu-Au–style mineralization occurs near the middle of the Navilawa Monzonite within an E–W belt centered on the Kingston prospect, 1.8 km north of the Tuvatu deposit [17]. Gold mineralization at Tuvatu and Banana Creek indicates a broad NE trend, which parallels the fault-controlled orientation of the Sabeto River (Figure 2). Stream-sediment and soil sampling by the Fijian Geological Survey and Barringer Fiji Ltd.(Toronto, ON, Canada) outlined a broad, weak

Cu anomaly at the southern end of the Navilawa Monzonite, as well as strong anomalies north of Kingston and at Nukulua Creek [17]. The Cu anomalies were strongest in the E–W belt centered on Kingston. Shoshonitic rocks contain up to 0.95% Cu over 10 m intervals, with most samples ranging from 16–4800 ppm Cu [17].
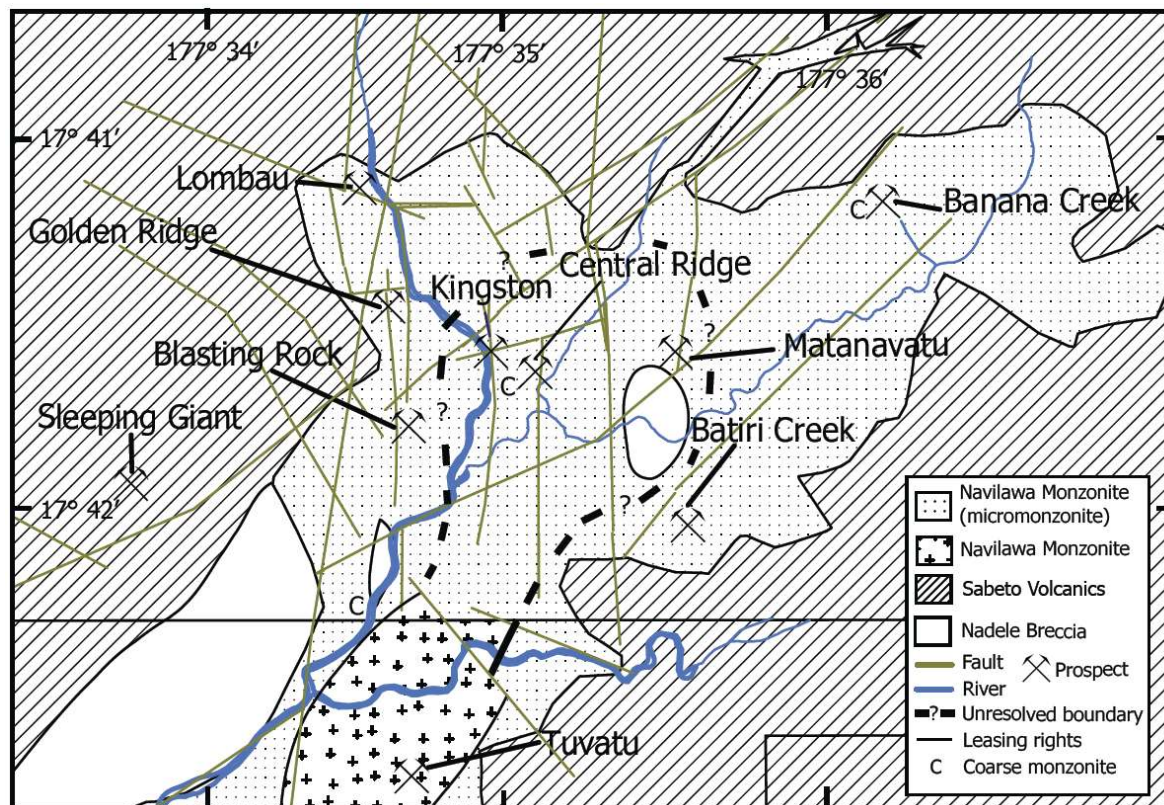
Figure 2. Simplified geologic map of the Navilawa caldera showing the location of the various porphyry Cu- and epithermal-style Au prospects. Drill hole locations are shown as 1 (TNDH001), 2 (TNDH002), 4 (TNDH004), 6 (BCDH6), 7 (BCDH7), and 8 (BCDH9).

Sampling by Continental Resources, aimed at assessing the gold potential near Kingston, discovered the best results at Central Ridge. Soil channel samples yielded 11 m at 4.45 g/t Au and 1.43% Cu, 14 m at 1.05 g/t Au and 1.04% Cu, and 12 m at 2.33 g/t Au [17]. Drilling completed at Central Ridge by Continental Resources identified broad, low-grade gold intersections, including the best interval of 12 m at 1.28 g/t Au [29].

The Banana Creek gold prospect is located within the Navilawa Monzonite and was discovered by conventional systematic drainage geochemistry and float mapping [17]. Individual veins are up to 50 cm wide and extend for up to 400 m [35]. Stream sediments recorded up to 0.26 g/t Au and rock-float sampling of quartz veins gave results ranging from 0.26 to 72.4 g/t Au, and averaging 6.2 g/t Au [33]. The predominant rock type is a fine- to medium-grained micromonzonite, which is cut by numerous dikes of trachyandesite and monzonite porphyry. These dikes trend NE with quartz veins locally occurring along their margins. Structures trending NNW were the result of later stages of faulting and shearing. Subsequent reactivation of the older NE structures is evident by another stage of coarse monzonite intrusions. The final stage of igneous activity involved an intrusion of unmineralized basalt dikes, which are considered to be equivalent to the Ba Volcanic Group [17,34].

3. Sampling and Analytical Methods

Two hundred and twenty three samples of Navilawa Monzonite and associated mineralization were collected from nine holes drilled by Golden Rim Resources Ltd. (Surrey Hills, Australia) and

surface outcrops. Drill hole locations were selected at porphyry- and epithermal-style mineralization within the Navilawa caldera at Banana Creek (BCDH6, BCDH7, BCDH8), Central Ridge (CDRH001, CDRH002, CDHRH003), and Tuvatu North (TNDH001, TNDH002, TNDH004). Some of these samples were used for petrographic and chemical analyses.

Eleven samples from drill cores BCDH6, BCDH7, and BCDH8 of unaltered to weakly altered monzonite were collected for major and trace element analysis. The major elements (SiO_2, Al_2O_3, Fe_2O_3, CaO, MgO, TiO_2, Na_2O, K_2O, MnO, P_2O_5, Cr_2O_3) were determined by $LiBO_2/Li_2B_4O_7$ fusion and measured by ICP–ES techniques, C and S by dry combustion analysis, and trace elements (Ba, Be, Pb, Co, Cs, Ga, Hf, Nb, Rb, Sn, Sr, Ta, Th, U, V, W, Zr, Y), including rare earth elements (La, Ce, Pr, Nd, Sm, Eu, Gd, Tb, Dy, Ho, Er, Tm, Yb, Lu), were obtained by $LiBO_2/Li_2B_4O_7$ fusion and measured by ICP–MS techniques by Acme Analytical Laboratories (Table 1). The standards used indicated accuracy to within ±5 ppm for trace elements and to within ±0.5 percent for major elements relative to an internal standard.

Table 1. Representative chemical composition of rock samples from the Banana Creek prospect. Values are in wt % for major elements and in ppm for trace elements except for Au, which is in ppb. Sample NF2 Cu value is shown as >X, which is >10,000 ppm. Samples NF2, NF6, and NF31 from drill hole BCDH8, NF73 from drill hole BCDH7, and NF100, NF106, NF115, and NF131 from drill hole BCDH6.

Rock Type	Monzonite								
Sample	NF2	NF6	NF31	NF73	NF100	NF106	NF108	NF115	NF131
SiO_2	47.94	48.72	48.41	50.55	47.69	48.6	47.68	48.74	46.69
TiO_2	0.7	0.62	0.66	0.53	0.79	0.62	0.73	0.55	0.64
Al_2O_3	15.79	19.25	16.07	17.2	16.39	15.92	15.31	17.04	15.57
Fe_2O_3	10.02	6.74	10.01	7.27	10.62	10.05	10.63	7.81	9.66
MnO	0.24	0.19	0.25	0.19	0.21	0.28	0.33	0.19	0.19
MgO	5.21	2.69	4.97	3.15	5.79	4.74	5.07	3.67	5.11
CaO	7.85	7.68	9.74	8.11	10.9	7.62	10.26	8.79	7.62
Na_2O	1.68	2.78	1.98	1.61	2.25	2.17	1.62	1.8	2.28
K_2O	4.42	3.99	4.33	6.63	2.22	5.39	5.03	5.57	3.96
P_2O5	0.48	0.56	0.47	0.41	0.32	0.5	0.56	0.42	0.5
LOI	4.1	6.6	3	4.1	2.6	3.9	2.7	5.2	7.6
TOT/C	0.1	0.68	0.12	0.3	0.22	0.41	0.34	0.54	1
TOT/S	0.02	0.03	0.12	0.03	0.02	0.13	0.07	1.1	2.09
Total	98.43	99.83	99.9	99.76	99.8	99.81	99.93	99.79	99.83
Ba	566.5	595.4	481.7	592.9	395.2	767.5	569	563.9	481.7
Cs	0.7	0.7	0.7	0.9	1.3	0.7	0.9	0.4	0.5
Hf	1.4	1.8	1.6	1.6	1.6	1.8	1.8	1.6	1.7
Nb	9.6	8	8.9	9.7	9.3	8.9	10.3	9.9	7.9
Ta	<0.1	0.1	0.1	0.1	<0.1	0.1	0.1	0.1	0.1
U	0.9	0.7	1	1.4	0.4	1.4	1	1.2	1.4
V	359	179	332	276	335	334	370	257	296
W	1.9	0.3	0.3	0.2	0.1	0.2	0.2	0.2	0.3
Y	18	15.2	18.3	18.1	15.5	17.1	19.7	15.9	18
La	12.2	7.5	13.5	14.7	4.7	14.2	14.2	13.3	14.6
Ce	24.5	17.1	28.5	29.8	11.2	31.2	32.2	26.7	31.2
Pr	3.49	2.33	3.91	4.03	1.62	4.14	4.49	3.49	4.23
Nd	16.6	10.7	17.8	17.9	8.2	19.3	20.6	15.6	19.8
Sm	4.1	2.7	4.6	4.2	2.3	4.8	5.4	3.8	4.7
Eu	1.26	0.83	1.27	1.24	0.82	1.28	1.55	1.12	1.4
Gd	3.98	2.74	4.19	3.69	2.63	4.19	4.76	3.36	4.28
Tb	0.64	0.47	0.68	0.61	0.51	0.66	0.76	0.54	0.67
Dy	3.28	2.6	3.37	3.17	2.62	3.24	3.74	2.91	3.49
Ho	0.59	0.49	0.62	0.58	0.53	0.56	0.67	0.64	0.62
Er	1.68	1.56	1.81	1.73	1.58	1.71	1.89	1.57	1.83
Tm	0.25	0.24	0.26	0.25	0.26	0.25	0.28	0.24	0.25

Table 1. *Cont.*

Rock Type	Monzonite								
Sample	NF2	NF6	NF31	NF73	NF100	NF106	NF108	NF115	NF131
Yb	1.59	1.58	1.72	1.71	1.52	1.61	1.77	1.55	1.69
Lu	0.23	0.24	0.25	0.25	0.24	0.25	0.26	0.23	0.26
Ag	1.5	<0.1	0.1	<0.1	<0.1	<0.1	<0.1	0.1	<0.1
As	<0.5	3.2	1.6	1.1	0.8	1.2	1.5	2.2	<0.5
Bi	<0.1	<0.1	0.2	<0.1	<0.1	0.1	<0.1	0.1	0.5
Cd	0.9	<0.1	0.2	0.1	<0.1	0.3	0.1	0.1	0.1
Cu	>X	276.2	264.7	159.8	187.3	160.3	190.3	153.2	330.8
Ga	15.1	15	14.6	15.1	14.6	14.4	16.2	14.1	14.7
Hg	0.01	0.01	<0.01	<0.01	<0.01	0.01	<0.01	0.02	0.01
Mo	0.3	1	0.7	0.2	1.1	0.5	0.4	0.3	1.4
Ni	9.6	6.8	10	3.4	14.8	11.3	9.3	6.5	13.2
Pb	3.3	3.4	4.4	8.8	1.9	10.2	7.4	4.3	8.3
Se	4.2	<0.5	0.9	0.5	<0.5	1.2	<0.5	<0.5	7.7
Sn	1	1	1	1	1	1	1	1	1
Tl	<0.1	<0.1	<0.1	<0.1	<0.1	0.1	<0.1	0.1	0.1
Zn	112	69	53	62	67	105	102	52	42

Electron microprobe analyses of silicates within the Navilawa Monzonite (n = 171) were obtained at the University of Minnesota using a JEOL 8900 electron probe microanalyzer. The operating conditions for the microprobe included an accelerating voltage of 15 kV, a beam current of 20 nA, and a beam spot size of 1–2 μm. The standards used included hornblende (Si, Al, Mg, Ca), ilmenite (Fe, Ti), albite (Al, Na), spessartine (Al, Mn), pyrope (Si, Mg), K-feldspar (K), gahnite (Al, Zn), tugtupite (Cl), vanadium metal (V), and apatite (F). The ZAF correction method was applied.

Twenty samples of pyrite from the Banana Creek prospect were analyzed for sulfur isotope compositions. Sulfide separates were cryogenically converted to SO_2 by combustion with vanadium oxide [36]. Data are reported in standard δ notation relative to the Vienna–Cnyon Diablo troilite (V–CDT) standard and all samples were analyzed with a Finnigan-MAT 252 stable isotope ratio mass spectrometer at Indiana University.

Thirty one samples of the most altered monzonite were collected for mineral identification by X-ray diffraction (XRD). Samples of rock were crushed, powdered, and sieved to <0.125 mm grain size. A 1M sodium acetate solution was added to 6 g of each sample and left to soak in a 40 °C water bath overnight to remove any carbonates. The samples were centrifuged and then treated with a 1 M NaCl solution three times, with centrifugation occurring after each wash. The suspensions were passed through a 53 μm sieve and placed in a reciprocating shaker overnight to achieve dispersion. Samples were centrifuged, washed with distilled water, and centrifuged again until settling stopped occurring. The clay solutions were dispersed further with a Misonix Sonicator 3000 and then centrifuged to allow grains >2 μm to settle.

Clay concentrations within the sample solutions were calculated to determine the appropriate volume to give 125 mg of clay. The clay minerals were mounted on ceramic tiles by a vacuum apparatus and treated with 20 mL each of 0.1 M $MgCl_2$ and distilled water. An application of a 50/50 glycerol solution was applied to the clay minerals and allowed to absorb before XRD analysis. The clay minerals were identified with a Siemens D5000 diffractometer at Iowa State University. Samples were analyzed from 0 to 32° 2θ at 2° 2θ/min, with Cu–Kα radiation. The XRD patterns were collected with VisXRD5000 software and peaks were matched to peaks in Table 5.18 of Brindley and Brown [37].

4. Petrochemistry of Igneous Rocks

4.1. Mineralogy

The Navilawa Monzonite contains approximately equal amounts of euhedral to subhedral plagioclase and potassium feldspar phenocrysts (0.10 to 2.5 mm in length), along with diopside (0.10

to 3.0 mm in length, Figure 3a), biotite, and magnetite (0.05 to 1.0 mm long). The groundmass consists mostly of tabular plagioclase and potassium feldspar that was partially to completely replaced by sericite, smectite, and illite. Diopside, biotite (Figure 3b), and apatite are also found in the groundmass, but identification is often made difficult due to the high degree of alteration. The basaltic–andesite dikes are composed of tabular diopside and plagioclase with lesser amounts of orthoclase and magnetite. Diopside contains 4.80–9.64 wt % FeO, 10.92–16.69 wt % MgO, 2.75–5.69 wt % Al_2O_3, and 0.16 to 0.95 wt % TiO_2 (Table 2).
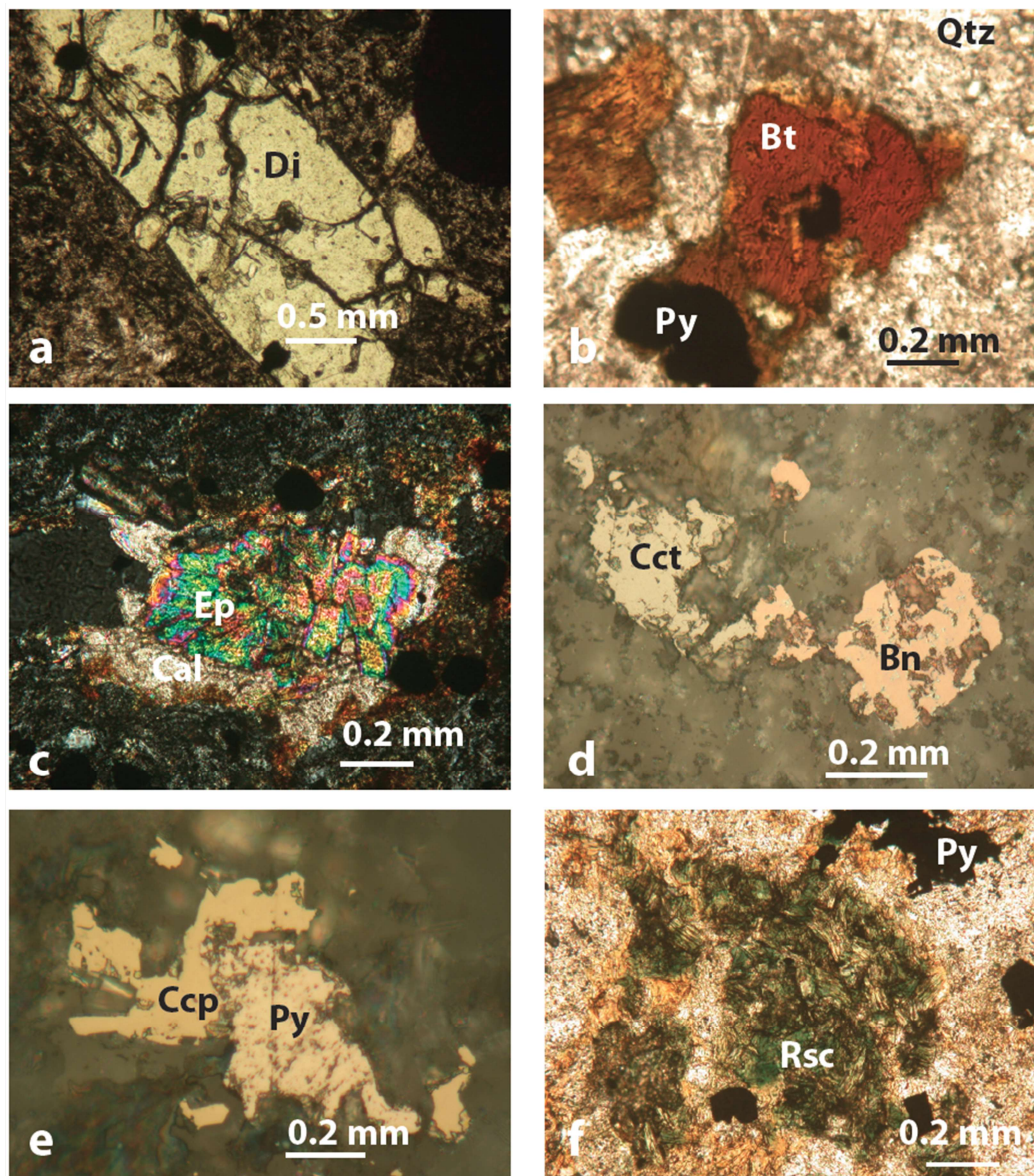
Figure 3. (**a**) Transmitted light (plane polarized) photomicrograph of diopside (Di) in typical monzonite in a fine-grained plagioclase matrix. (**b**) Transmitted light (plane polarized) photomicrograph of biotite (Bt) and pyrite (Py) in moderately altered monzonite. (**c**) Transmitted light (cross polarized) photomicrograph of propylitic alteration consisting of epidote (Ep) and calcite (Cal) in micromonzite, Central Ridge Cu prospect. (**d**) Reflected light (plane polarized) image of chalcocite (Cct) and bornite (Bn), Central Ridge Cu prospect. (**e**) Reflected light (plane polarized) image of chalcopyrite (Ccp) and pyrite (Py) in the Banana Creek prospect. (**f**) Transmitted light (plane polarized) image of roscoelite (Rsc) and pyrite (Py) in phyllic alteration, Banana Creek. Mineral abbreviations are after Whitney and Evans [38] except for roscoelite, which was not included in their study.

Table 2. Representative electron microprobe analyses of silicates from the Banana Creek prospect. Sample NF21 is from drill hole BCDH8, samples NF73, NF75 from drill hole BCDH7, and samples NF106, NF108, NF117, and NF123B from drill hole BCDH6.

	1	2	3	4	5	6	7	8
wt %	NF117	NF108	NF106	NF73	NF123B	NF21	NF75	NF123B
SiO_2	37.26	36.40	48.08	49.23	37.58	38.57	30.13	31.75
TiO_2	0.15	0.08	0.23	0.47	3.21	3.86	0.05	1.53
Al_2O_3	22.53	23.14	1.90	4.67	15.91	16.48	17.92	15.58
V_2O_3	0.92	0.00	1.18	0.09	0.39	0.00	0.00	0.17
FeO	12.76	13.09	4.80	7.59	14.00	12.81	18.56	25.15
MnO	0.60	0.60	0.11	0.28	0.18	0.25	1.18	0.13
MgO	0.12	0.05	16.67	13.03	17.67	17.07	18.85	12.86
ZnO	0.07	0.01	0.00	0.03	0.12	0.06	0.10	0.04
CaO	25.39	24.83	25.87	25.44	0.15	0.10	0.27	0.50
K_2O	0.00	0.01	0.00	0.01	7.25	8.77	0.04	0.12
F	0.00	0.00	0.00	0.00	0.03	0.00	0.01	0.00
Cl	0.01	0.00	0.01	0.00	0.23	0.06	0.01	0.19
Total	99.79	98.21	98.84	100.83	96.64	98.02	87.11	87.97
apfu								
Si	5.795	5.748	7.305	7.347	5.929	5.998	5.276	5.652
Ti	0.017	0.010	0.027	0.053	0.380	0.452	0.006	0.205
Al	4.130	4.308	0.340	0.821	2.958	3.021	3.699	3.269
V	0.115	0.000	0.143	0.010	0.049	0.000	0.000	0.025
Fe	1.659	1.728	0.609	0.947	1.847	1.666	2.719	3.744
Mn	0.080	0.080	0.014	0.036	0.024	0.034	0.176	0.019
Mg	0.027	0.012	3.776	2.899	4.156	3.956	4.919	3.411
Zn	0.008	0.001	0.000	0.003	0.014	0.007	0.013	0.005
Ca	4.231	4.202	4.211	4.067	0.026	0.017	0.051	0.095
K	0.000	0.001	0.001	0.001	1.458	1.740	0.009	0.028
F	0.002	0.000	0.000	0.000	0.015	0.002	0.003	0.000
Cl	0.004	0.000	0.002	0.001	0.062	0.017	0.003	0.058
Total	16.066	16.090	16.428	16.185	16.917	16.910	16.873	16.510

1, 2 epidote; 3, 4 diopside; 5, 6 biotite; 7, 8 chlorite; apfu–atoms per formula unit.

Coarse-grained compositionally zoned biotite occurs in samples of Navilawa Monzonite adjacent to the Tuvatu deposit [10,30]. However, biotite studied here in monzonite elsewhere within the Navilawa caldera is medium to dark brown in color and shows no compositional or optical zoning. Magmatic biotite is Mg-rich (16.22–20.22 wt % MgO) and contains lesser amounts of Fe (8.84–15.63 wt % FeO), along with a high TiO_2 content (2.03–4.37 wt %) (Table 2).

Chlorite is variable in composition but is generally Mg-rich (11.22–20.19 wt % MgO) and contains 13.63 to 28.56 wt % FeO, and up to 1.25 wt % V_2O_3. Epidote that coexists with chlorite and calcite in propylitic alteration varies in composition with FeO contents ranging from 9.26 to 15.78 wt % (Figure 3c). Up to 0.69 wt % V_2O_3 is also present in epidote.

4.2. Major and Trace Element Whole-Rock Geochemistry

The majority of the igneous rocks from the Navilawa caldera are weakly to strongly altered; the least altered samples were chosen for trace element analysis. Monzonite contains 46.7 to 50.5 wt % SiO_2, and 4.4 to 8.2 wt % $Na_2O + K_2O$, where $K_2O > Na_2O$. Based on a total alkali–silica diagram [39], monzonites fall within the alkaline field defined by Miyashiro [40], and are chemically equivalent to volcanic rocks consisting of trachybasalts, basaltic trachyandesites, tephrites/basanites, phonotephrite, and tephriphonolite (Figure 4a). Data from Scherbarth and Spry [10] on basaltic–andesite dikes at Tuvatu are included for comparative purposes and plot within the sub-alkaline field, consisting of

basalt, basaltic–andesite, trachy–basalt and phonotephrite. Samples of monzonite from the Tuvatu and Banana Creek prospects occupy positions in the shoshonite and ultrapotassic fields (Figure 4b).
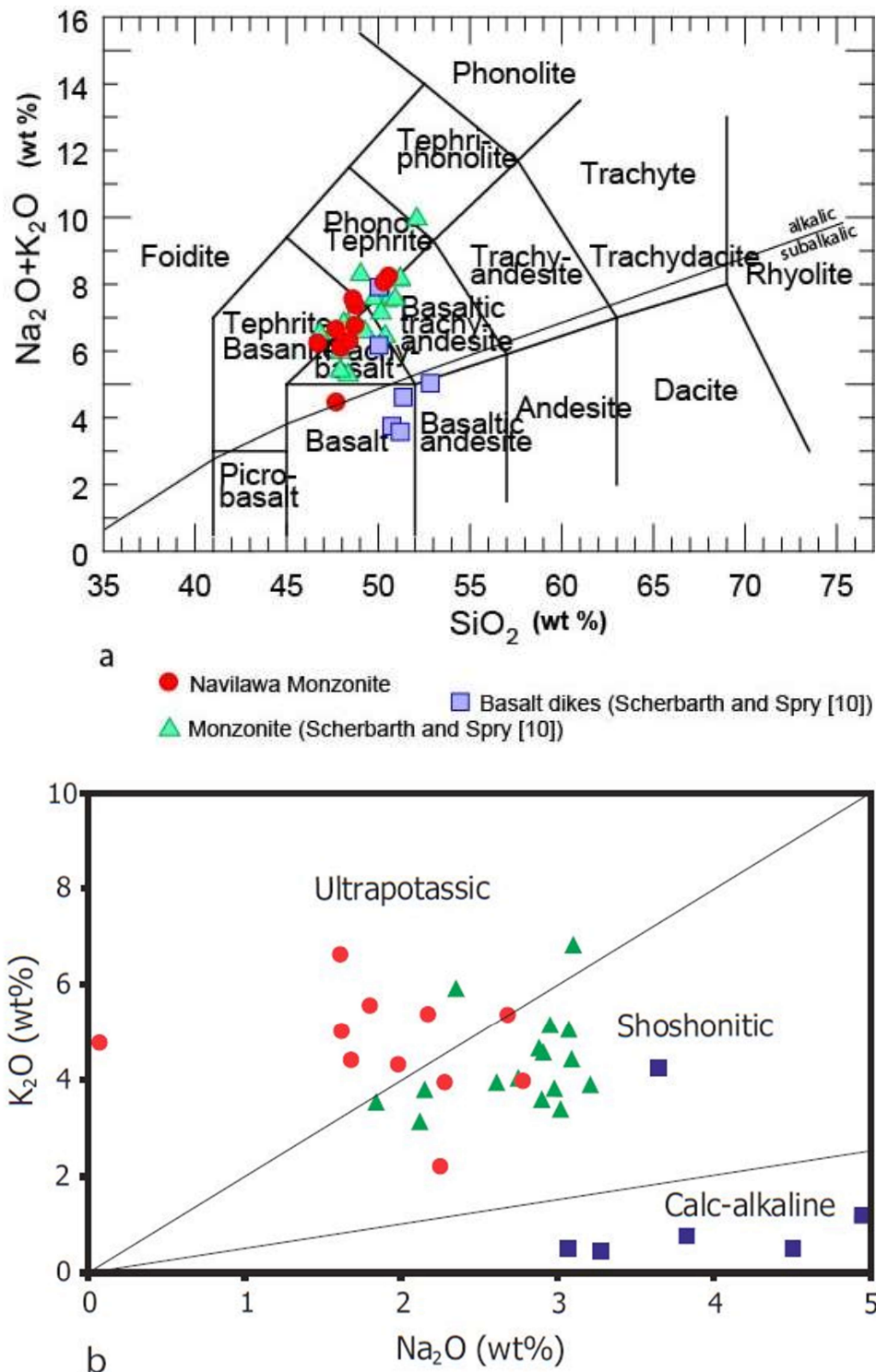
Figure 4. (**a**) Total alkali–silica diagram of Le Bas et al. [39] for Navilawa Monzonite from the Navilawa caldera. The alkalic–subalkalic line is also shown [40]. (**b**) Plot of K_2O (wt. %) versus Na_2O (wt. %) showing the fields of ultrapotassic, shoshonitic and calc–alkaline fields [41,42]. Data from the Navilawa Monzonite and basaltic–andesite dikes from the Tuvatu prospect taken from Scherbarth and Spry [10].

Monzonites within the Navilawa caldera exhibit moderate to weak negative correlations between TiO_2 ($r^2 = 0.51$), MgO ($r^2 = 0.40$), Fe_2O_3 ($r^2 = 0.34$), and CaO ($r^2 = 0.24$) concentrations versus SiO_2 content. The concentrations of Al_2O_3 ($r^2 = 0.20$), and K_2O ($r^2 = 0.45$) exhibit weak positive correlations with SiO_2 content. Data from Scherbarth and Spry [10] show comparable negative and positive correlations and similar trace element patterns to monzonites within the caldera, suggesting that monzonites have the same magma source.

These correlations, along with a calc–alkaline trend (Figure 5), reflect the early fractionation of ferromagnesian silicates and oxides and the later fractionation of plagioclase, orthoclase, and biotite. By comparison, discrimination diagrams for the basaltic–andesite dikes suggest that they were not derived from the same magma that formed the monzonites [10].
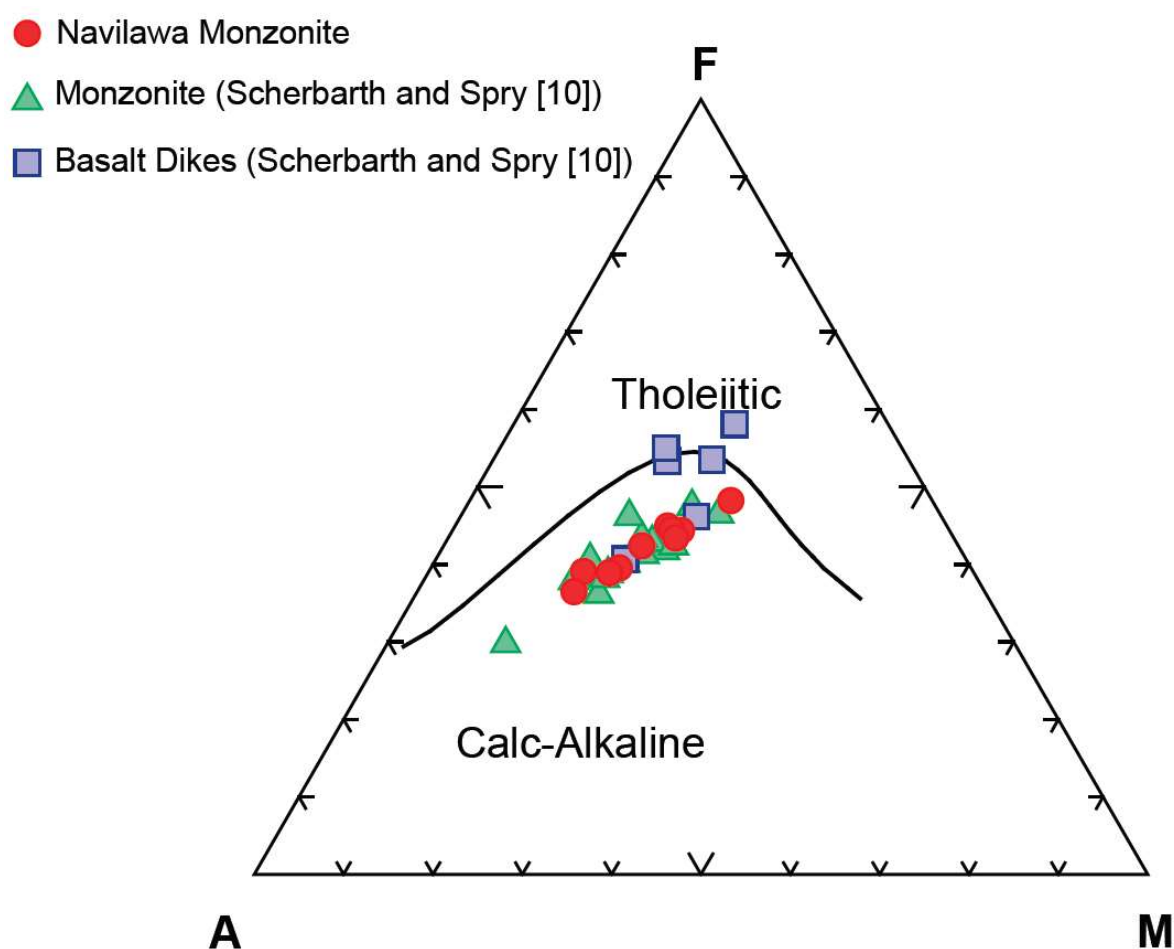
Figure 5. AFM diagram of the Navilawa Monzonite from this study and Scherbarth and Spry [10] along with basaltic–andesite dikes from [10]. A = $Na_2O + K_2O$, F = Fe_2O_3*0.8998, M = MgO.

The Cu, Pb, and Zn contents of the Navilawa Monzonite in the caldera are variable: 153.2–1765.4 ppm Cu (mean = 375 ppm), 1.9–10.2 ppm Pb (mean = 5 ppm), and 42–112 ppm Zn (mean = 71 ppm) (Table 1). These values are very similar to those obtained by Scherbarth and Spry [10] for monzonite from the Tuvatu deposit (25–869 ppm Cu, 2–11 ppm Pb, and 28–177 ppm Zn). Shoshonites adjacent to the Emperor deposit contain 7–23 ppm Pb [43], whereas alkalic intrusive rocks associated with the Porgera gold deposit (Papua New Guinea) contain 14–133 ppm Cu, 4–42 ppm Pb, and 58–127 ppm Zn [5], and diorites related to the Escondida Cu deposit, Chile, contain 6–80 ppm Cu and 32–99 ppm Zn [44]. It should also be noted that the V content of monzonite near the center of the Navilawa caldera (179–359 ppm) is similar to the range of V (235–465 ppm) reported by Spry and Scherbarth [45].

Chondrite-normalized rare earth element (REE) patterns and spider diagrams for the Navilawa Monzonite located in the caldera and the Tuvatu deposit show very similar enrichments and depletions. The REE patterns of the monzonite from this study, as well as data from Scherbarth and Spry [10], are light rare earth element (LREE) enriched and heavy rare earth element (HREE) depleted and show no Eu anomalies (Figure 6). The basaltic–andesite dikes, in contrast, show flat REE patterns and weakly negative Eu anomalies [10]. The shape of the REE patterns for the Navilawa Monzonite is similar to those of other alkalic rocks from Fiji [46], those adjacent to the Porgera gold deposit, Papua New Guinea [5], and shoshonitic rocks from Limnos, Greece [47]. Pe-Piper et al. [47] proposed that a LREE-enrichment and HREE-depletion pattern can only be explained by partial melting of an enriched metabasaltic amphibolite in the absence of significant garnet. A spider diagram of the Navilawa and Tuvatu monzonites and basaltic–andesite dikes strongly suggests an island arc source due to the negative Nb anomaly with respect to Th and Ce, the depletion of Ta, Zr, Hf, and Ti, and K enrichment accompanied by high concentrations of Sr (828.6–2329.4 ppm), Ba (395–767.5 ppm), and Rb (37.5–113 ppm) (Figure 7). The shape of the patterns resembles those for other Fijian shoshonitic rocks [26], and is comparable to the shoshonitic lavas from the Tavua volcano adjacent to the Emperor deposit [43].
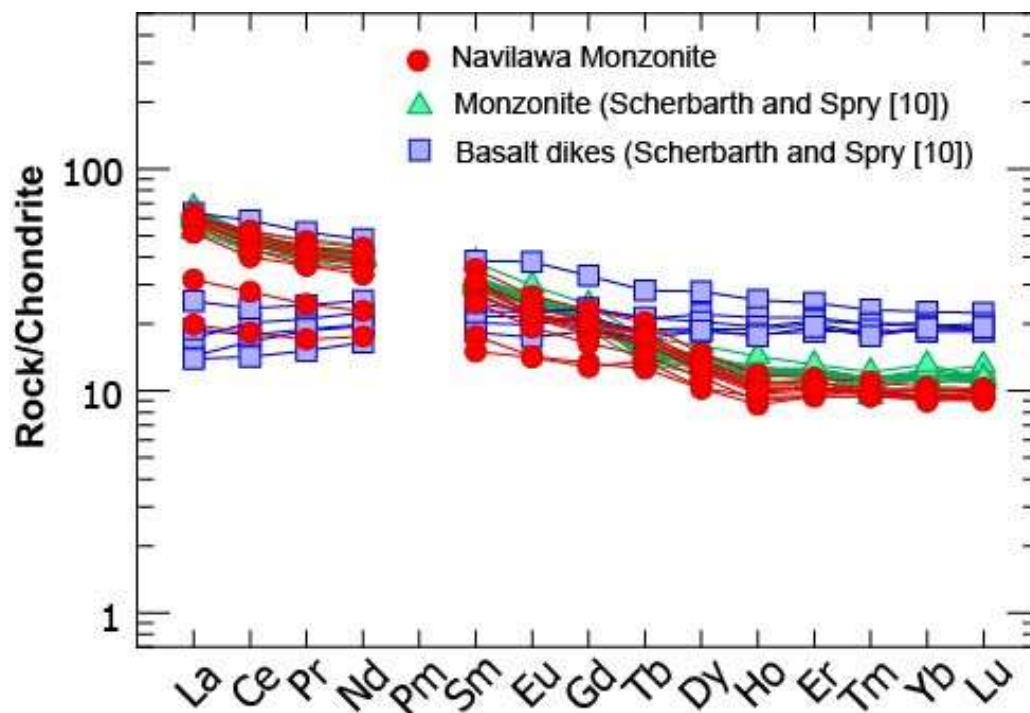
Figure 6. Chondrite-normalized REE patterns of the Navilawa Monzonite and basaltic–andesite dikes from the Tuvatu prospect. Data from the Navilawa Monzonite and basaltic–andesite dikes from the Tuvatu prospect taken from Scherbarth and Spry [10]. Normalization values are from Anders and Grevesse [48] and multiplied by 1.36 to maintain consistency with the older ordinary chondrite normalization values.
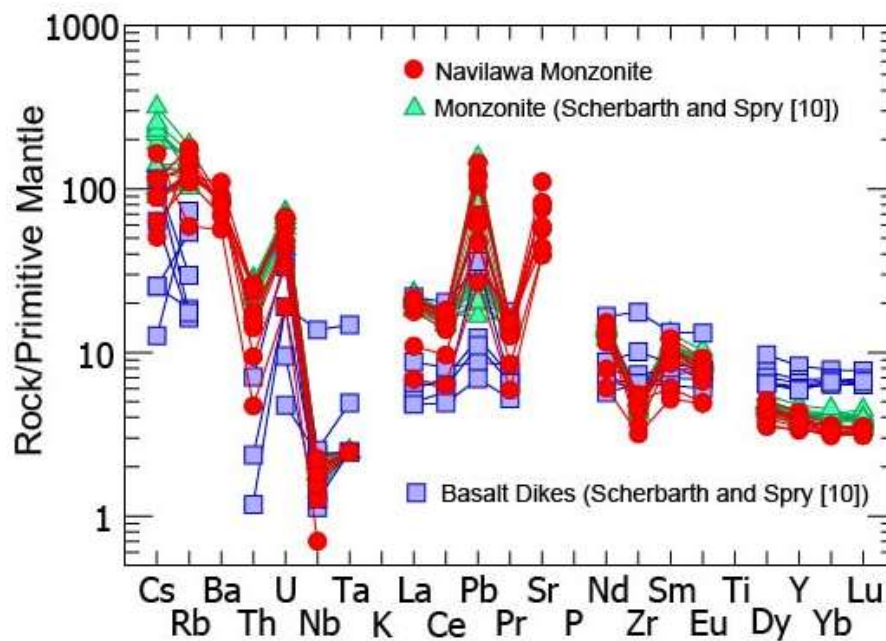
Figure 7. Mantle-normalized trace element patterns for Navilawa Monzonite. Data from Navilawa Monzonite and basaltic–andesite dikes from the Tuvatu prospect are from Scherbarth and Spry [10]. Normalization values are from Sun and McDonough [49]].

5. Porphyry- and Epithermal-Style Mineralization

5.1. General Description

Porphyry and epithermal mineralization occurred with the emplacement of the Navilawa Monzonite and movement along the Viti Levu lineament. The epithermal mineralization formed as a series of N–S trending veins and south-dipping flatmakes at the Tuvatu deposit [10], which strike northeastward into the caldera.

The mineralization in the Navilawa caldera occurs as thin (0.5–2 cm) veinlets within the Navilawa Monzonite and surrounded by narrow alteration halos. Veins in the Kingston porphyry Cu–Au deposit and Central Ridge area are commonly calcitic with lesser amounts of quartz, epidote and chlorite filling voids between the calcite (Figure 3c). Sulfides and oxides associated with the porphyry stage consist of disseminated magnetite and chalcopyrite and trace amounts of pyrite, bornite, chalcocite, and covellite. Secondary malachite and chrysocolla are also present (Figure 8a). Aside from the presence of minor chalcocite (Figure 3d) and covellite replacement of chalcopyrite and bornite along grain boundaries or in fractures, samples examined optically and by XRD analyses show very little evidence of supergene alteration. Unlike chalcopyrite and bornite, other sulfides (pyrite, sphalerite, and galena) show no evidence of replacement by other minerals.

By contrast, epithermal mineralization consists primarily of dense quartz, adularia, calcite, and pyrite veins (Figure 8b,c). Pyrite and chalcopyrite are also abundant as disseminations (Figure 3e), whereas sphalerite is only associated with veins (Figure 8d) and is less common than pyrite or chalcopyrite. Trace amounts of galena and inclusions of hematite in pyrite appear in epithermal mineralization as well.
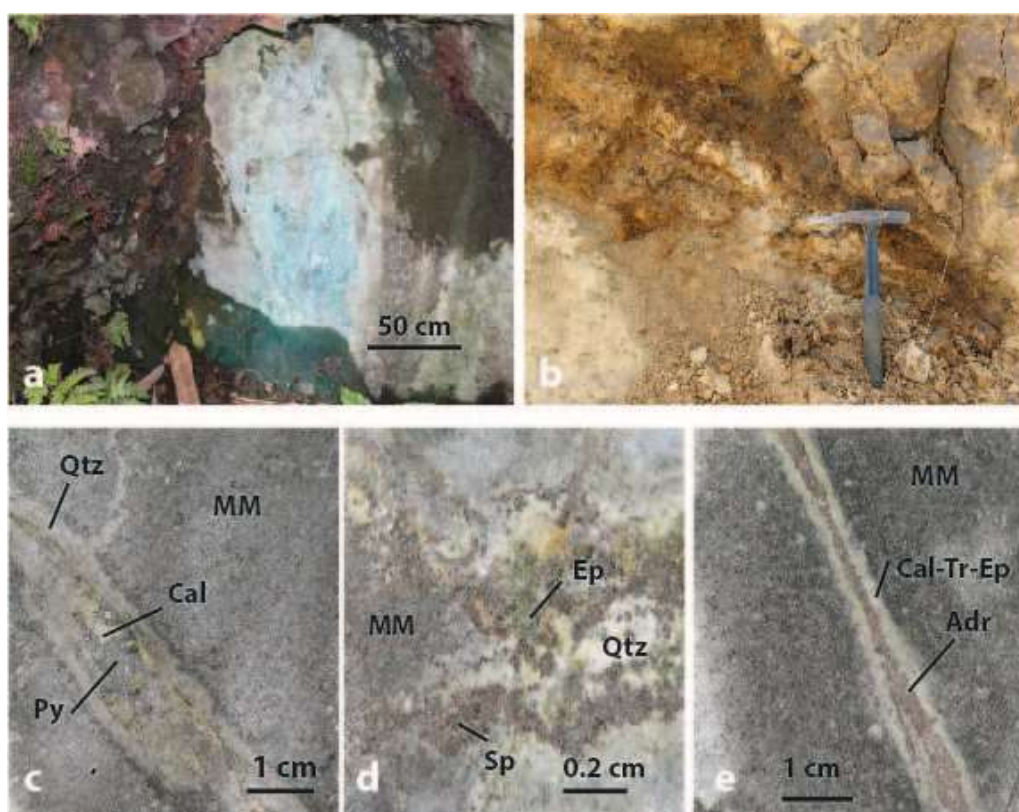
Figure 8. Photographs of (**a**) Kingston Cu-Au prospect portal showing green secondary intergrown malachite and azurite. (**b**) Quartz and pyrite in the Ilie vein (Banana Creek prospect). (**c**) Quartz (Qtz)–calcite (Cal)–adularia–pyrite vein in micromonzonite (MM) in the Banana Creek prospect. (**d**) Patch of quartz (Qtz), epidote (Ep), and sphalerite (Sp) in micromonzonite in the Banana Creek prospect. (**e**) Andradite (Adr) vein in micromonzonite surrounded by a rim of intergrown calcite-tremolite (Tr)–epidote in the Tuvau North prospect. Mineral abbreviations are after Whitney and Evans [38].

5.2. Alterations

5.2.1. Porphyry-Style

Both porphyry- and epithermal-styles of mineralization occur in the Tuvatu deposit, with alteration associated with porphyry style mineralization being dominated by potassic alteration (orthoclase, and biotite), whereas the epithermal-style mineralization is characterized by phyllic alteration (quartz, sericite, pyrite, adularia, roscoelite (Figure 3f), tourmaline, and minor amounts of V-oxides and silicates), with lesser amounts of propylitic alteration (epidote, chlorite) [10,45]. The same types of alteration assemblages are pervasive through the Navilawa Monzonite in the caldera, but the most intense alteration occurs in the bleached halos adjacent to veinlets. Propylitic alteration (chlorite, calcite, epidote, quartz) is the dominant assemblage in samples from the Kingston and Central Ridges prospects and it, along with phyllic alteration (quartz, sericite, pyrite, smectite, and illite), appears to have overprinted potassic alteration (potassium feldspar, secondary biotite, and actinolite) and the primary magmatic mineralization. The potassic alteration is the most difficult to discern due to the overprinting by later alteration stages and the shared mineralogy with the magmatic stage from the Kingston and Central Ridges deposit. Magnetite and chalcopyrite are the best indicators of potassic alteration in samples that appear to be least affected by propylitic alteration. Chlorite is the most prominent propylitic alteration mineral, which partially to completely replaced diopside, feldspar, and biotite so only relict grain boundaries are visible. Chlorite is variable in appearance; colors range from translucent to dark green and shapes range from radial fans to anhedral masses. Epidote and calcite typically fill veins or vugs as anhedral to subhedral grains in this assemblage.

Phyllic alteration associated with porphyry style mineralization has a more limited spatial distribution compared to the propylitic alteration. The assemblage commonly appears as disseminated subhedral quartz grains and sericitic replacement of feldspars. The groundmass of samples with phyllic alteration is typically altered to smectite or illite, making primary mineral identification impossible in heavily altered samples. This is the first stage where pyrite forms as disseminations or intergrowths with chalcopyrite. Magnetite from the potassic and propylitic stages is locally replaced by pyrite.

5.2.2. Epithermal-Style

Propylitic alteration at the Tuvatu North (TNDH004) prospect contained orange-brown anhedral to subhedral dodecahedrons of andraditic garnets in association with calcite, epidote, and chlorite. Tremolite, epidote, and calcite also accompany andradite-bearing veins (Figure 8e), forming as anhedral grains that fill voids between the garnets. Phyllic alteration associated with the Banana Creek and Tuvatu North prospects is dominated by quartz, adularia, pyrite, sericite, illite, and smectite. In Banana Creek samples, pyrite appears as disseminations and in veins along with quartz and adularia. Sericite typically replaces feldspars or forms adjacent to pyrite or quartz grains. Samples from Tuvatu North show a more intense epithermal assemblage compared to Banana Creek. Quartz–adularia and pyrite-filled veins that include sphalerite and galena are typical with adularia being replaced by sericite and other clay mineral. Hematite is present as inclusions in pyrite or as tiny disseminations.

Minerals common to supergene alteration, such as kaolinite, halloysite, alunite, and jarosite, also do not appear optically in thin section or as peaks in XRD samples.

5.2.3. Phyllosilicate Minerals Associated with Epithermal Veins

Thirty one samples were selected to identify the phyllosilicates in alteration zones spatially associated with epithermal mineralization in the Tuvatu North (TNDH001, TNDH002, and TNDH004) and Banana Creek prospects (BCDH6, BCDH7, and BCDH8).

X-ray diffraction analyses show the presence of chlorite, which is consistent with the dominant propylitic alteration visible in thin sections (Figures 9 and 10). Corrensite $[(Mg,Fe)_9(Si,Al)_8O_{20}(OH)_{10} \cdot nH_2O]$ was also identified in samples from three Banana Creek drill cores (Figure 11) and drill core TNDH004 from Tuvatu North (Figure 10). Corrensite appears in samples at depth (100–170 m) in Banana Creek and Tuvatu North, with the exception of BCDH6 where it is present in all samples examined starting at a depth of 49 m. The corrensite found in TNDH004 (Figure 10) from 99 to 149 m is located in the same samples that contain andradite.

Samples from the Tuvatu North prospect, TNDH001 and TNDH002 (Figure 10), show smectite peaks at a range of depths, occurring as shallow as 30 m and as deep as 272 m. The samples of intense propylitic alteration that contain corrensite show very small smectite peaks, possibly as a result of the transformation of saponite to corrensite. Phyllosilicates in Banana Creek samples BCDH6 and BCDH7 (Figure 11) also mirror this trend with samples in each drill core showing intense smectite peaks where corrensite is not present at a depth of 78–103 m and weak or no peak where corrensite peaks appear (49 m, 131–170 m). Fluid inclusion studies of quartz from the Tuvatu deposit reported that propylitic ore fluids had homogenization temperatures ranging from 205 to 382 °C [10]. The temperature range indicates that smectite and corrensite probably formed during the later stages of hydrothermal activity.

Illite appears in drill cores TNDH001, TNDH002, and BCHD8 from 45 to 110 m (Figures 10 and 11), with one sample at a depth of 185 m. Feldspar and clinopyroxene are the likely precursors to illite alteration [19]. Fluids giving rise to phyllic alteration are typically meteoric in origin, although the assemblage is probably the result of interactions between meteoric fluids and potassic or propylitic alteration. Illite in hydrothermal systems is typically stable from 230 to 320 °C [19], which is consistent with its formation in the Banana Creek prospect based on the studies of Ricketts et al. [34] in which fluid inclusions homogenized at ~260 °C. Other porphyry/epithermal deposits (e.g., Campana Mahuida, Argentina; Favona, New Zealand) report similar temperatures for phyllic stage and/or illite alteration at 190–290 °C [21] and 150–220 °C [23].
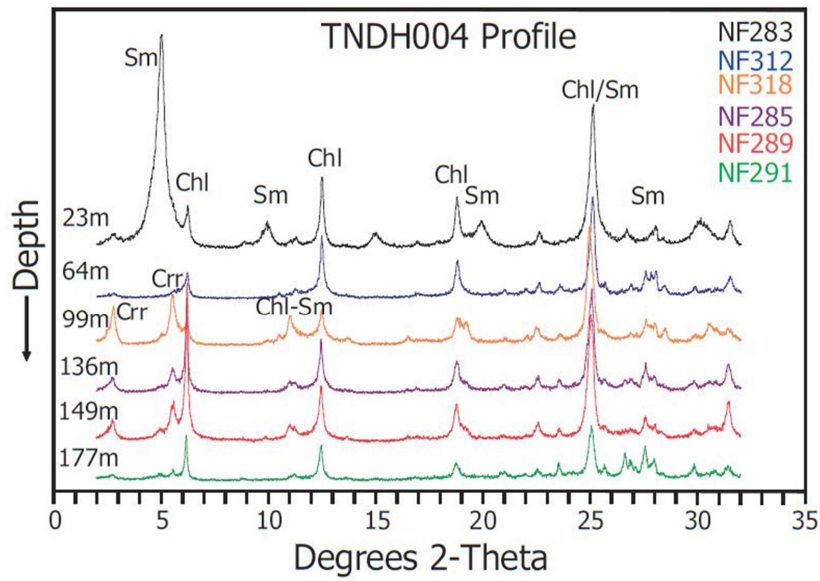
Figure 9. X-ray diffraction profiles showing the presence of various phyllosilicates including chlorite (Chl), smectite (Sm), corrensite (Crr), and illite (Ill), in samples NF283, NF312, NF318, NF285, NF289, and NF291 at depths of 23 m, 64 m, 99 m, 136 m, 149 m, and 177 m, respectively, in drill hole TNDH004 (Tuvatu North prospect).
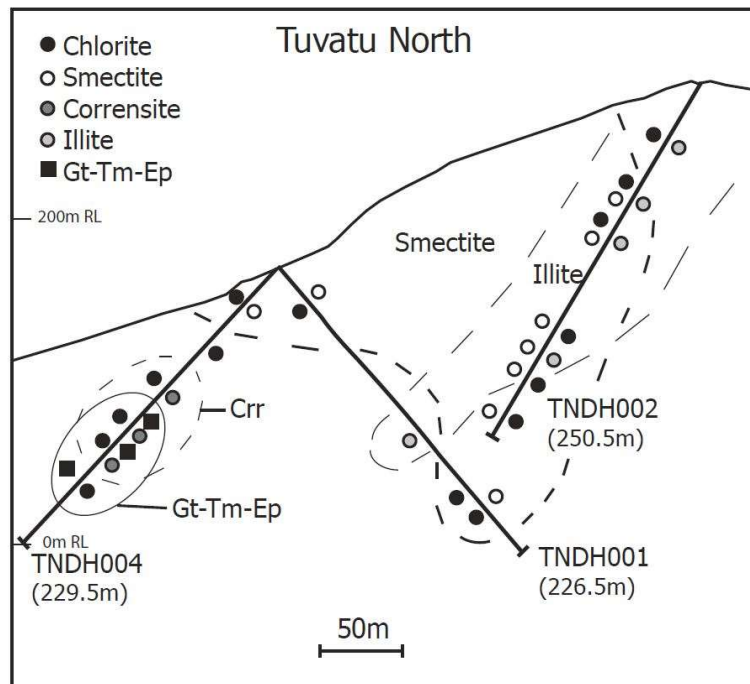
Figure 10. Cross-section through the Tuvatu North prospect showing drill holes TNDH001, TNDH002, and TNDH004 and the down-hole distribution of alteration minerals: smectite, illite, corrensite (Crr), garnet (Gt), tremolite (Tm), and epidote (Ep). The length of the drill holes is also indicated.
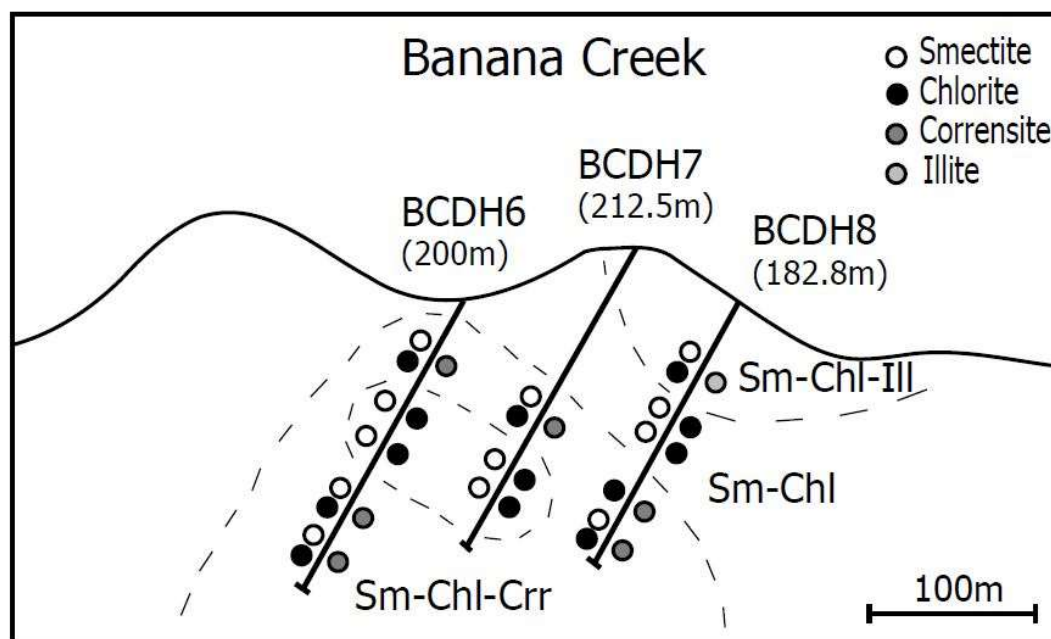
Figure 11. Cross-section through the Banana Creek prospect showing drill holes BCDH6, BCDH7, and BCDH8 and the down-hole distribution of alteration minerals: smectite, illite, corrensite, and chlorite. The length of the drill holes is also indicated.

5.2.4. Alteration Geochemistry

Twenty eight of the samples used for XRD analysis were also used to determine major (SiO_2, Al_2O_3, Fe_2O_3, CaO, MgO, TiO_2, Na_2O, K_2O, MnO, P_2O_5, and Cr_2O_3) and trace element (Ba, Ni, Sr, Zr, Y, Nb, and Sc) compositions of the host rocks to evaluate the intensity of alteration that occurred in the Navilawa Monzonite. The alteration index, AI = $100(MgO + K_2O)/(MgO + K_2O + CaO + Na_2O)$ [50], reflects the replacement of plagioclase by sericite, illite, and chlorite during hydrothermal alteration. The index was originally developed for altered felsic volcanic rocks hosting volcanic-hosted massive sulfide deposits, but Gemmell and Large [51] showed that it was applicable for any hydrothermal alteration in intermediate to mafic volcanic rocks. The chlorite–carbonate–pyrite index, CCPI = $100(MgO + FeO)/(MgO + FeO + K_2O + Na_2O)$, measures the degree of chlorite, carbonate and pyrite alteration [52]. A plot of AI versus CCPI, which was referred to by Large et al. [52] as the "alteration box plot", gives the relationship of the whole rock geochemistry to alteration mineralogy and extent of metasomatism. Within the alteration zones, the more intensely altered samples plot toward the compositions of end-member alteration minerals (albite, K feldspar, sericite, chlorite, dolomite, ankerite, and epidote), whereas least-altered volcanic rocks plot toward the center of the diagram (Figure 12).
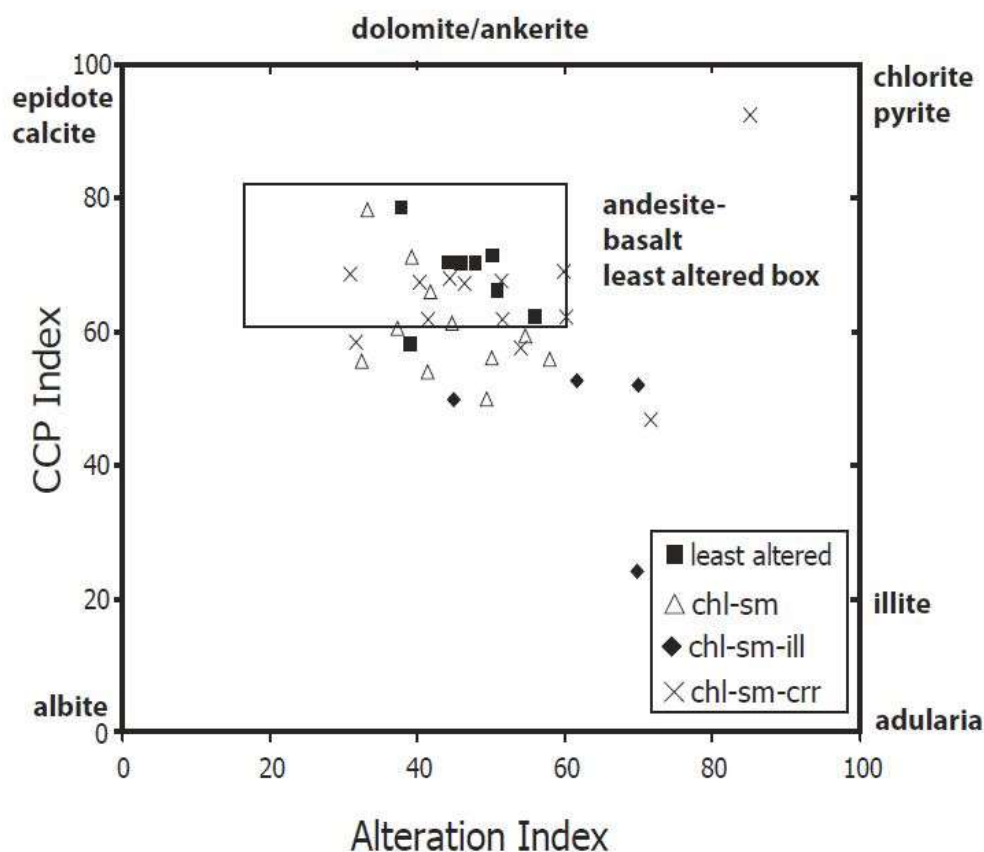
Figure 12. Alteration box plot showing samples collected from least altered and altered rocks. Altered samples dominated by chlorite (chl)–smectite (sm), chlorite–smectite–illite (ill), and chlorite–smectite–corrensite (corr) are indicated along with least-altered andesite-basalt box.

Altered and least-altered Navilawa Monzonite samples plot in the alteration box towards the upper center of the diagram (Figure 12). Most of the least-altered samples plot within the andesite/basalt box [52]. Propylitic alteration is the dominant assemblage in samples from the Navilawa caldera and as a result, these samples plot in the least-altered box because alteration to epidote, Fe chlorite, and albite does not change the whole rock composition of the fresh rock [22]. Plotting within the least-altered box may also indicate that the propylitic alteration was more regional in scale, although there is evidence of vein-related propylitic alteration, particularly at Tuvatu North. Propylitic samples with a greater proportion of chlorite and carbonate result in higher CCPI and AI values, which explains the outlier near the chlorite end member. The variability in plots of the illite samples is likely due to varying intensity of illitic alteration compared to the more uniform compositions obtained for samples that were subject to propylitic alteration.

5.3. Sulfide Mineralogy and Sulfur Isotopes

Pyrite is by far the most abundant sulfide in the Navilawa caldera. The Tuvatu deposit contains abundant pyrite, which hosts native gold and tellurides [10]. In samples from Tuvatu North, pyrite shows a variety of textures, typically a variation of disseminated grains formed as fine-grained (0.1–0.4 mm) pyritohedrons, subhedral cubes, or singular blades. Occasional anhedral to subhedral pyritohedrons occur in quartz and calcite veins or large (1–3 mm) subhedral cubes and pyritohedrons in pyrite-filled veins. Pyrite at Tuvatu North contains fine-grained (<0.1–0.4 mm) inclusions of anhedral chalcopyrite, pyrrhotite, or bladed hematite, whereas pyrite from Banana Creek appears much more uniform in texture. Pyrite occurs as anhedral to subhedral cubic grains or pyritohedrons (<0.1–0.4 mm) in association with quartz and calcite veins or as disseminations hosted within the wall rock. Pyrite

from this area contains inclusions of chalcopyrite or magnetite and, in some cases, has been included in magnetite.

Tuvatu North also hosts minor amounts of sphalerite, galena, bornite, chalcocite, and covellite, which do not appear at Banana Creek in the drill holes evaluated here in any significant amounts. Anhedral sphalerite (0.1–1.5 mm) occurs in quartz–adularia veins and commonly displays intergrowths with pyrite and chalcopyrite. Galena is locally present as 0.25–3 mm size anhedral grains in quartz–calcite veins, whereas bornite formed as a replacement of chalcopyrite or as fine-grained anhedral disseminations (0.1–0.9 mm in size). Chalcocite and covellite are present along grain boundaries and fractures in bornite, which is likely due to minor supergene alteration. Although specific tellurides were not identified by Mears [35], he reported a Au–As–Hg–Te association based on the geochemistry of rock chips and float samples. No precious metal tellurides were identified here. Twenty samples of pyrite in veinlets from the Banana Creek prospect were analyzed for sulfur isotope compositions and have values of $\delta^{34}S$ = −6.2 to +0.4 per mil (Figure 13).
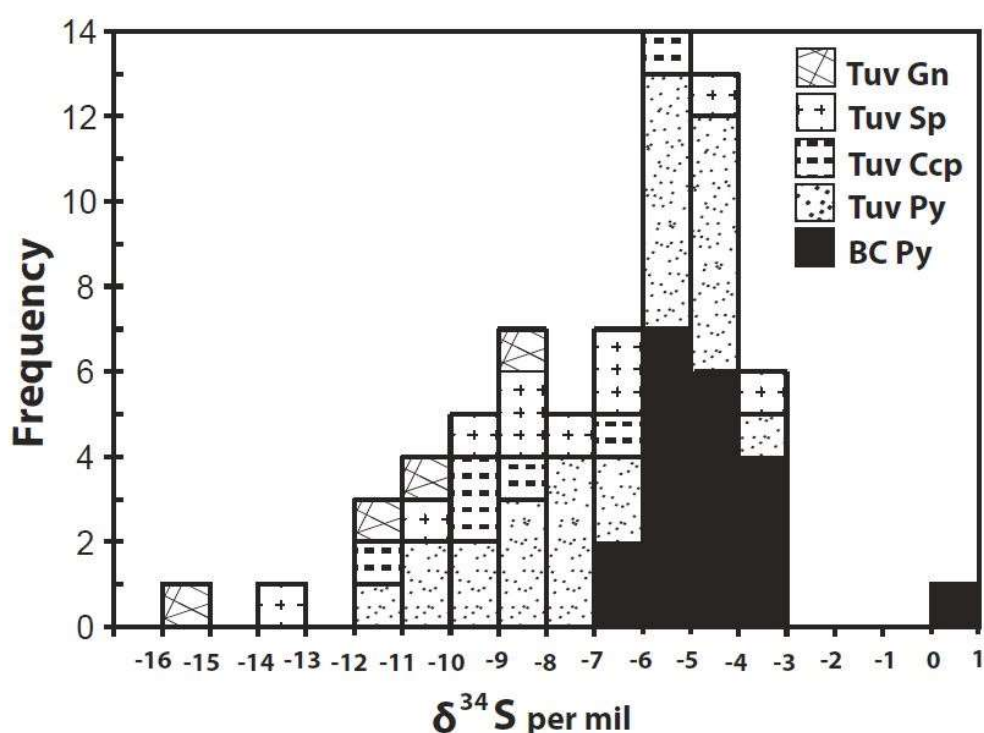
Figure 13. Histogram of $\delta^{34}S$ compositions of pyrite from the Banana Creek (BC Py; this study) and galena (Gn), sphalerite (Sp), chalcopyrite (Ccp), and pyrite (Py) for epithermal veins from the Tuvatu prospect (data from [10]).

6. Discussion

The source of sulfur and other metals is likely from the Navilawa Monzonite given that the Navilawa caldera contains no sedimentary rocks. The $\delta^{34}S$ values of pyrite from the Banana Creek prospect fall within the range of magmatic sulfur values [53] and typical porphyry copper deposits. Scherbarth and Spry [10] reported $\delta^{34}S$ values (−11.7 to −3.2 per mil) for pyrite at Tuvatu whereas Ahmad et al. [9] and Begg [11] reported ranges of sulfur isotopes for sulfides from the Emperor deposit of $\delta^{34}S$ = −15.3 to −4.2 per mil and −20 to +3.9 per mil, respectively. The low isotope values for each deposit is likely due to phase separation of the ore fluid, which created volatile H_2S relative to SO_2 and as a result caused an increase in fO_2. The direct addition of magmatic volatiles to hydrothermal fluids can also create these low values. Temperatures below 400 °C will cause SO_2 to disproportionate from volcanic gases into reduced and oxidized species, resulting in sulfides becoming enriched in ^{32}S relative to H_2SO_4 [54]. Such disproportionation of SO_2 is common in epithermal gold deposits

(e.g., [55]). The evolution from porphyry to epithermal-style fluids is important to the precipitation of precious and base metals. Increases in pH or fO_2 during phase separation will result in the gold solubility to decrease, which will cause gold to precipitate [11]. Evidence for phase separation at Emperor and Tuvatu is based on fluid inclusion observations of Begg [11] and Scherbarth and Spry [10], respectively. In addition, calculations made by Spry and Scherbath [45] for the assemblage calaverite–roscoelite–karelianite in the epithermal stage at Tuvatu is supportive of high fO_2 conditions. Fluid inclusions quartz at Banana Creek [34], which contain native gold, chalcopyrite, sphalerite, and galena, homogenized at around 260 °C. Although phase separation was not reported in these inclusions, quartz formed after platy calcite, which is commonly associated with precipitation from boiling fluids through exsolution of CO_2 [56].

Fluid inclusion data from Tuvatu suggest that the hydrothermal fluids evolved from a high-temperature (>500 °C) and high-salinity (>50 wt % NaCl equiv) porphyry stage to a moderate temperature (80–330 °C) and salinity (~8 wt % NaCl equiv) epithermal stage [10]. The hydrothermal fluids circulating within the Navilawa caldera likely had appreciable concentrations of dissolved CO_2 in order to form calcite, epidote and other calc-silicates. The formation of hydrothermal clays is generally temperature dependent with illite and smectite forming at temperatures greater than 220 to less than 150 °C [23]. This range of temperatures is consistent with that proposed by Rickets et al. [34] for the alteration assemblage they reported from the Banana Creeks prospect of smectite–halloysite/kaolinite at around 150–200 °C. Diopside and K-feldspar within the Navilawa Monzonite were the likely precursors to smectite and illite during the propylitic and phyllic stages of alteration. Metasomatism of Fe + Mg and Fe + Ca produced favorable conditions for the formation of saponite and andradite [57], respectively. It should be noted that anomalous concentrations of andradite occur in the alteration zones of porphyry Cu deposits (e.g., Escondida, Chile, [58]) and in many surficial types of sediment spatially associated with porphyry deposits in the Atacama Desert, Chile. Andradite is considered to be an indicator mineral for these porphyry Cu deposits due to the chemical composition closely matching the Fe + Ca metasomatism that characterizes propylitic alteration, as well as its stable and easily-identifiable nature [57].

Studies of marine hydrothermal systems at Pantelleria caldera, Italy [59], Tonga Trench, Tonga [60], Betic Cordilleras, Spain [61,62], and Mururora Atoll, French Polynesia [63] and synthesis experiments [64] have demonstrated that saponite [$Ca_{0.25}(Mg,Fe)_3(Si,Al)_4O_{10}(OH)_2 \cdot nH_2O$] will convert to corrensite at hydrothermal temperatures. Abad et al. [61] reported corrensite formation at 200–270 °C. Hydrothermally altered basalts from Middle Atlas, Morocco also indicate corrensite formation occurred at 200 °C to <350 °C [65]. In each of the studies, the temperature of hydrothermal activity and permeability of the host rocks played an important role in corrensite formation, and they likely account for its formation within the Navilawa caldera and why it is more common in the Banana Creek samples where fracturing and dike intrusion is particularly common. X-ray diffraction analysis also showed the presence of smectite of the saponite–beidellite group, although compositions were not determined (Figures 9–11). Saponite was previously reported under varying physicochemical conditions from supergene weathering to rocks found at zeolite grade [65]. An alteration study of monzonites at the Bingham Canyon porphyry Cu deposit (Utah) suggests that smectite formed at 200 to 220 °C [20]. Saponite and corrensite formation has been reported to have a genetic relationship with Ca-rich silicates [23,61,62].

The occurrence of corrensite also supports some degree of saponite formation in the Navilawa caldera due to the transformational relationship between the two minerals [59–64]. The spatial association of corrensite with propylitic assemblages (andradite, tremolite, calcite, epidote, and chlorite), fluid inclusion data from quartz in propylitic alteration at Tuvatu (205–382 °C [10]), and suggested temperatures of formation for saponite and corrensite (e.g., [61,65]) indicate that saponite/corrensite formation occurred in the Navilawa caldera during the propylitic stage and also possibly in the phyllic stage.

Diopside in dolerite in the Betic Cordilleras was reported as the precursor to saponite alteration [62] while Abad et al. [61] argued that saponite alteration occurring in host marly rocks was the result of a period of contact metamorphism that formed diopside, andradite, vesuvanite, and titanite. The Ca-rich nature of the magmatic and propylitic assemblages in the Navilawa caldera is the likely precursor to saponite formation as well, although other smectite compositions cannot be ruled out. Trioctahedral saponitic as well as dioctahedral smectites of the bedellite-montmorillonite series are commonly produced in hydrothermal alteration of mafic rocks [62]. Parry et al. [20] reported smectite in monzonite porphyry, concluding it represented a constituent of intermediate argillic alteration.

The pervasive nature of propylitic alteration in the Tuvatu caldera, which consists of chlorite, calcite, and epidote that replaced diopside and K-feldspar phenocrysts or occurred as void fillings suggests that hydrothermal fluids remained fairly stagnant while interacting with these silicates. In contrast, andradite, calcite, and tremolite is completely confined to the margins of veins at Tuvatu North, which suggests that this type of propylitic alteration was fracture-controlled. It appears the intensity of the propylitic assemblage that formed was dependent on faults and fractures to serve as fluid conduits, whereas pervasive alteration relied on diffusive flow through the monzonite. The alteration of the porphyry system at the Tavua caldera appears comparable to that at the Navilawa caldera as Begg [11] identified similar andradite–calcite veining along with widespread propylitic and/or phyllic alteration along the Crown Jewel Fault in the Emperor deposit.

The clay minerals within the Navilawa caldera show very little evidence of zoning in the Tuvatu North or Banana Creek samples; the presence of epithermal veins superimposed on the pervasive propylitic assemblage, as well as the paragenetic sequence developed for Tuvatu [10], indicates overlapping alteration occurred as hydrothermal activity progressed. Similar overprinting of the epithermal lode alteration upon low-temperature propylitic alteration has been described at the Emperor deposit [11,19].

7. Conclusions

Alkaline igneous rocks of the Navilawa caldera host the Tuvatu low-sulfidation epithermal gold deposit, porphyry copper–gold-style mineralization and several other epithermal gold veins, including the Banana Creek and Tuvatu North prospects. Although porphyry- and epithermal-styles of mineralization is telescoped in the Tuvata deposit over hundreds of meters, there is a greater physical separation between these styles of mineralization elsewhere in the Navilawa caldera. Potassic, propylitic, and phyllic alteration occur throughout the Navilawa caldera with phyllic alteration being most closely associated with epithermal gold mineralization. Diffuse propylitic alteration occurs throughout the caldera and is most intense where spatially associated with porphyry- and epithermal-style mineralization.

Monzonites of the Navilawa and Tavua calderas have similar compositions and were erupted during the early stages of the destruction of the Vanuatu–Fiji–Tonga arc following intra-arc collision. The compression of the Viti Levu lineament in northwestern Viti Levu resulted in the formation of low-grade porphyry Cu and epithermal gold mineralization in both the Tavua and Navilawa calderas. The overlapping range of sulfur isotopic compositions for metallic mineralization at Emperor, Tuvatu, and Banana Creek suggests a magmatic source of sulfur from the spatially associated shoshonitic volcanic rocks in both calderas. These isotopic compositions, the temperature of gold formation (as based on the previous fluid inclusion studies and the stability of clay minerals), coupled with the presence of pyrite and hematite in the gold-bearing veins, indicates that the ore fluid in the Banana Creek and Tuvatu North prospects was oxidizing, near the hematite–pyrite buffer, and at neutral pH conditions.

Similarities in composition of the alkaline igneous rocks of almost identical age in the Navilawa and Tavua calderas, and the presence of both low-grade porphyry Cu and epithermal Au–(Te) mineralization in both calderas highlights the potential presence of a large gold telluride system in the Navilawa caldera, in addition to the gold resource in the Tuvatu prospect. There are strong geological similarities between the metallic mineralization in the Navilawa caldera and elsewhere in the SW Pacific Ocean at the Emperor, Porgera, Acupan, Mt. Kare, and Ladolam deposits. These similarities include the transition from porphyry Cu- to low-sulfidation epithermal-style Au–Te mineralization, the geologic setting, the composition of the igneous rocks, and the precious metal mineralogy and attendant alteration [4,6–8].

Author Contributions: N.A.F. and P.G.S. collected the samples. N.A.F. and M.L.T. obtained and evaluated the X-ray diffraction data while P.G.S. obtained and evaluated the electron microprobe data. The manuscript was written by N.A.F. and P.G.S.

Conflicts of Interest: The authors declare no conflict of interest.

References

1. Richards, J.P. Petrology and geochemistry of alkalic intrusives at the Porgera gold deposit, Papua New Guinea. *J. Geochem. Expl.* **1990**, *35*, 141–199. [CrossRef]
2. Jensen, E.P.; Barton, M.D. Gold deposits related to alkaline magmatism. *Rev. Econ. Geol.* **2000**, *13*, 279–314.
3. Kelley, K.D.; Spry, P.G. Critical metals associated with alkaline-rock related epithermal gold deposits. *Rev. Econ. Geol.* **2016**, *18*, 195–216.
4. Cooke, D.R.; McPhail, D.C. Epithermal Au-Ag-Te mineralization, Acupan, Baguio district, Philippines; numerical simulations of mineral deposition. *Econ. Geol.* **2001**, *96*, 109–132.
5. Richards, J.P. Alkalic-type epithermal gold deposits, a review. *Mineral. Assoc. Can. Short Course Ser.* **1995**, *23*, 367–400.
6. Richards, J.P.; Kerrich, R. The Porgera gold mine, Papua New Guinea: Magmatic hydrothermal to epithermal evolution of an alkalic-type precious metal deposit. *Econ. Geol.* **1993**, *88*, 1017–1052. [CrossRef]
7. Richards, J.P.; Ledlie, I. Alkalic intrusive rocks associated with the Mount Kare gold deposit, Papua New Guinea: Comparison with the Porgera intrusive complex. *Econ. Geol.* **1993**, *88*, 755–782. [CrossRef]
8. Carman, G.D. Geology, mineralization, and hydrothermal evolution of the Ladolam gold deposit, Lihir Island, Papua New Guinea. *Soc. Econ. Geol. Spec. Pub.* **2003**, *10*, 247–284.
9. Ahmad, M.; Solomon, M.; Walsh, J.L. Mineralogical and geochemical studies of the Emperor gold telluride deposit, Fiji. *Econ. Geol.* **1987**, *82*, 345–370. [CrossRef]
10. Scherbarth, N.L.; Spry, P.G. Mineralogical, petrological, stable isotope, and fluid inclusion characteristics of the Tuvatu gold-silver telluride deposit, Fiji: Comparisons with the Emperor deposit. *Econ. Geol.* **2006**, *101*, 135–158. [CrossRef]
11. Begg, G. Genesis of the Emperor Gold Deposit, Fiji: Unpub. Ph.D. Thesis, Monash University, Clayton, Australia, 1996.
12. Begg, G. Gold and tectonics: A dynamic link. In Proceedings of the Ores and Ore Genesis 2007: Circum-Pacific Tectonics, Geologic Evolution, and Ore Deposits Symposium, Tucson, AZ, USA, 24–30 September 2007; Prog. Abst., No. 108.
13. Begg, G.C.; Loucks, R.R.; Gray, D.R.; Foster, D.A.; Kent, A.J.; Cooke, D.R. Magmas, fluids, and tectonics: The Emperor story. *Geol. Soc. Aust. Abst.* **1997**, *44*, 7.
14. Begg, G.; Gray, D.R. Arc dynamics and tectonic history of Fiji based on stress and kinematic analysis of dikes and faults of the Tavua Volcano, Viti Levu Island, Fiji. *Tectonics* **2002**, *21*, 1–14. [CrossRef]

15. JICA-MMAJ. *Report on the Cooperative Mineral Exploration in the Viti Levu Area, the Republic of Fiji. Phase I*; Metal Mining Agency of Japan Report, report number 91-41; Japan International Cooperation Agency: Tokyo, Japan, 1991.

16. JICA-MMAJ. *Report on the Cooperative Mineral Exploration in the Viti Levu Area, the Republic of Fiji. Phase I*; Metal Mining Agency of Japan Report, report number 92-082; Japan International Cooperation Agency: Tokyo, Japan, 1992.

17. Colley, H.; Flint, D.J. *Metallic Mineral Deposits of Fiji*; Memoir; no. 4; Fiji Mineral Resources Department: Suva, Fiji, 1995.

18. Setterfield, T.N.; Mussett, A.E.; Oglethorpre, R.D.J. Magmatism and associated hydrothermal activity during the evolution of the Tavua caldera: ^{40}Ar-^{39}Ar dating of the volcanic intrusive, and hydrothermal events. *Econ. Geol.* **1992**, *87*, 1130–1140. [CrossRef]

19. Eaton, P.C.; Setterfield, T.N. The relationship between epithermal and porphyry hydrothermal systems within the Tavua Caldera, Fiji. *Econ. Geol.* **1993**, *88*, 1053–1083. [CrossRef]

20. Parry, W.; Jasumback, M.; Wilson, P. Clay mineralogy of phyllic and intermediate argillic alteration at Bingham, Utah. *Econ. Geol.* **2002**, *97*, 221–239. [CrossRef]

21. Franchini, M.; Impiccini, A.; Meinert, L.; Grathoff, G.; Schalamuk, I.B.A. Clay mineralogy and zonation in the Campana Mahuida porphyry Cu deposit, Neuquén, Argentina: Implications for porphyry Cu exploration. *Econ. Geol.* **2007**, *102*, 27–54. [CrossRef]

22. Gemmell, J.B. Hydrothermal alteration associated with the Gosowong epithermal Au-Ag deposit, Indonesia: Mineralogy, geochemistry, and exploration implications. *Econ. Geol.* **2007**, *102*, 893–922. [CrossRef]

23. Simpson, M.P.; Mauk, J.L. The Favona epithermal gold-silver deposit, Waihi, New Zealand. *Econ. Geol.* **2007**, *102*, 817–840. [CrossRef]

24. Bongiolo, E.M.; Patrier-Mas, P.; Mexias, A.S.; Beaufort, D.; Formoso, M.L.L. Spatial and temporal evolution of hydrothermal alteration at Lavras do Sul, Brazil: Evidence of dioctahedral clay minerals. *Clays Clay Min.* **2008**, *56*, 222–243. [CrossRef]

25. Hamburger, M.W.; Isacks, B.L. Diffuse back-arc deformation in the southwestern Pacific. *Nature* **1988**, *332*, 599–604. [CrossRef]

26. Gill, J.B.; Whelan, P. Early rifting of an oceanic island arc (Fiji) produced shoshonitic to tholeiitic basalts. *J. Geophys. Res.* **1989**, *94*, 4561–4578. [CrossRef]

27. Hathaway, B. The Nadi Basin: Neogene strike-slip faulting and sedimentation in a fragmental arc, Western Viti Levu, Fiji. *J. Geol. Soc. Lond.* **1993**, *150*, 563–581. [CrossRef]

28. Scherbarth, N.L. Petrological, Mineralogical, Fluid Inclusion and Stable Isotope Characteristics of the Tuvatu Gold-Silver Telluride Deposit, Upper Sabeto River, Fiji: Unpub. Master's Thesis, Iowa State University, Ames, IA, USA, 2002.

29. Ricketts, C.B.; Johnson, D.W. *Annual Report for Period Ending 30 June 1988, SPL 1218: Continental Resources (Fiji) Ltd Report 88/35*; Fiji Mineral Resources Department: Suva, Fiji, 1988; Unpublished work.

30. Hatcher, R. Relation of Structures, Alteration and Mineralisation at the Tuvatu Gold Prospect, Viti Levu, Fiji islands. Unpublished Bachelor's Thesis, Queensland Institute of Technology, Brisbane, Australia, 1998.

31. Rodda, P. Outline of the geology of Viti Levu, Fiji. New Zealand. *J. Geol. Geophys.* **1967**, *10*, 1260–1273. [CrossRef]

32. McDougall, I. Potassium-argon ages of some rocks from Viti Levu, Fiji. *Nature* **1963**, *198*, 677. [CrossRef]

33. A-Izzeddin, D. The Tuvatu Gold Project, Western Viti Levu. In Proceedings of the Pacific Exploration Technology (PET 98) Conference, Nadi, Fiji, September 1998; pp. 29–30.

34. Ricketts, C.B.; Johnson, D.W.; Lemcke, D.J. *Annual Report for the Period to 30 June 1989, SPL 1218: Continental Resources (Fiji) Ltd Report 88/73*; Fiji Mineral Resources Department: Suva, Fiji, 1989; Unpublished work.

35. Meares, R.M.D. *Annual Report for the Period 30 June 1990. Continental Resources (Fiji) Ltd Report 90/28. Fiji Mineral Resources Department Exploration Report 1218-9*; Fiji Mineral Resources Department: Suva, Fiji, 1990.

36. Yanagisawa, F.; Sakai, H. Thermal decomposition of barium sulfate-vanadium pentoxide-silica glass mixtures for preparation of sulfur dioxide isotope ratio measurements. *Anal. Chem.* **1983**, *55*, 985–987. [CrossRef]

37. Brindley, G.W.; Brown, G. *Crystal Structures of Clay Minerals and Their X-ray Identification*; Mineralogical Society of Great Britain and Ireland: Middlesex, UK, 1980; Volume 5, ISBN 9780903056373.

38.   Whitney, D.L.; Evans, B.W. Abbreviations for names of rock-forming minerals. *Am. Mineral.* **2010**, *95*, 185–187. [CrossRef]

39.   Le Bas, M.J.; Le Maitre, R.W.; Streickeisen, A.; Zanettin, B. A chemical classification of volcanic rocks based on total alkali-silica diagram. *J. Petrol.* **1986**, *27*, 745–750. [CrossRef]

40.   Miyashiro, A. Nature of alkalic volcanic rock series. *Contr. Mineral. Petrol.* **1978**, *66*, 91–104. [CrossRef]

41.   Peccerillo, A.; Taylor, S.R. Geochemistry of the Eocene calc-alkaline volcanic rocks in the Kastamonu area, northern Turkey. *Contr. Mineral. Petrol.* **1976**, *90*, 63–81. [CrossRef]

42.   Foley, S.F.; Venturelli, G.; Green, D.H.; Toscani, L. The ultrapotassic rocks: Characterization, classification, and constraints for petrogenetic models. *Earth Sci. Rev.* **1987**, *24*, 81–134. [CrossRef]

43.   Rogers, N.W.; Setterfield, T.N. Potassium and incompatible-element enrichment in shoshonitic lavas from the Tavua volcano, Fiji. *Chem. Geol.* **1994**, *118*, 43–62. [CrossRef]

44.   Richards, J.P.; Boyce, A.J.; Pringle, M.S. Geologic evolution of the Escondida area, Northern Chile: A model for spatial and temporal localization of porphyry Cu mineralization. *Econ. Geol.* **2001**, *96*, 271–305. [CrossRef]

45.   Spry, P.G.; Scherbarth, N.L. Vanadium silicates and oxides in the Tuvatu gold-silver telluride deposit, Fiji. *Mineral. Petrol.* **2006**, *87*, 171–186. [CrossRef]

46.   Morrison, G.W. Characteristics and tectonic setting of the shoshonite rock association. *Lithos* **1980**, *13*, 97–108. [CrossRef]

47.   Pe-Piper, G.; Piper, D.J.W.; Koukouvelas, I.; Dolansky, L.M.; Kokkalas, S. Postorogenic shoshonitic rocks and their origin by melting underplated basalts: The Miocene of Limnos, Greece. *Geol. Soc. Am. Bull.* **2009**, *121*, 39–54. [CrossRef]

48.   Anders, E.; Grevesse, N. Abundance of elements. Meteoritic and solar. *Geochim. Cosmochim. Acta* **1989**, *53*, 197–214. [CrossRef]

49.   Sun, S.-S.; McDonough, W.F. Chemical and isotopic systematics of ocean basalts: Implications for mantle composition and processes. *Geol. Soc. London Spec. Pub.* **1989**, *42*, 313–345. [CrossRef]

50.   Ishikawa, Y.; Sawaguchi, T.; Iwaya, S.; Horiuchi, M. Delineation of prospecting targets for Kuroko deposits based on modes of volcanism of underlying dacite and alteration halos. *Mining Geol.* **1976**, *26*, 105–117.

51.   Gemmell, J.B.; Large, R.R. Stringer system and alteration zones underlying the Hellyer volcanic-hosted massive sulfide deposit, Tasmania, Australia. *Econ. Geol.* **1992**, *87*, 620–649. [CrossRef]

52.   Large, R.R.; Gemmell, J.B.; Paulick, H.; Huston, D.L. The alteration box plot: A simple approach to understanding the relationship between alteration mineralogy and lithogeochemistry associated with volcanic-hosted massive sulfide deposits. *Econ. Geol.* **2001**, *96*, 957–971. [CrossRef]

53.   Ohmoto, H. Stable isotope geochemistry of ore deposits. *Rev. Mineral.* **1986**, *16*, 491–559.

54.   Ohmoto, H.; Rye, R.O. Isotopes of sulfur and carbon. In *Geochemistry of Hydrothermal Ore Deposits*, 2nd ed.; Barnes, H.L., Ed.; John Wiley and Sons: Hoboken, NJ, USA, 1979; pp. 509–567.

55.   Arribas, A., Jr. Characteristics of high sulfidation epithermal deposits and their relation to magmatic fluid. In *Magmas, Fluids, and Ore Deposits*; Short Course Series; Thompson, J.F.H., Ed.; Mineralogical Association of Canada: Nepean, ON, Canada, 1995; Volume 23, pp. 419–454.

56.   Simmons, S.F.; Christenson, B.W. Origins of calcite in a boiling geothermal system. *Am. J. Sci.* **1994**, *294*, 361–400. [CrossRef]

57.   Averill, S.A. Viable indicators in surficial sediments for two major base metal deposit types: Ni-Cu-PGE and porphyry Cu. In Proceedings of the 24th International Applied Geochemistry Symposium Indicator Mineral Methods in Mineral Exploration, Workshop B, Fredericton, NB, Canada, 1–4 June 2009.

58.   Padilla Garza, R.A.; Titley, S.R.; Pimentil, B.F. Geology of the Escondida porphyry copper deposit, Antofagasta region, Chile. *Econ. Geol.* **2001**, *96*, 307–324. [CrossRef]

59.   Fulignati, P.; Malfitano, G.; Sbrana, A. The Pantelleria caldera geothermal system: Data from the hydrothermal minerals. *J. Volc. Geoth. Res.* **1997**, *75*, 251–270. [CrossRef]

60.   Vitali, F.; Blanc, G.; Larqué, P.; Duplay, J.; Morvan, G. Thermal diagenesis of clay minerals within volcanogenic material from the Tonga convergent margin. *Marine Geol.* **1999**, *157*, 105–125. [CrossRef]

61.   Abad, I.; Jiménez-Millán, J.; Molina, J.M.; Nieto, F.; Vera, J.A. Anomalous reverse zoning of saponite and corrensite caused by contact metamorphism and hydrothermal alteration of marly rocks associated with subvolcanic bodies. *Clays Clay Mins.* **2003**, *51*, 543–554. [CrossRef]

62.   Jiménez-Millán, J.; Abad, I.; Nieto, F. Contrasting alteration processes in hydrothermally altered dolerites from the Betic Cordillera, Spain. *Clay Mins.* **2008**, *43*, 267–280. [CrossRef]

63. Mas, A.; Meunier, A.; Beaufort, D.; Patrier, P.; Dudoignon, P. Clay minerals in basalt-hawaiite rocks from Mururora Atoll (French Polynesia). I. Mineralogy. *Clays Clay Mins.* **2008**, *56*, 711–729. [CrossRef]

64. Roberson, H.E.; Reynolds, R.C., Jr.; Jenkins, D.M. Hydrothermal synthesis of corrensite: A study of transformation of saponite to corrensite. *Clay Clay Mins.* **1999**, *47*, 212–218. [CrossRef]

65. Dekayir, A.; Amouric, M.; Olives, J. Clay minerals in hydrothermally altered basalts from Middle Atlas, Morocco. *Clay Mins.* **2005**, *40*, 67–77. [CrossRef]